

Master of Science in Automotive Engineering

Faculty of Engineering



**POLITECNICO
DI TORINO**

Final Thesis and Dissertations

Experimental Setup to Measure the State of Charge and State of Health of Lead Acid Batteries

Supervisor: Prof. Andrea Tonoli

Co-Supervisor: Prof. Dr. Luis Arturo Gómez Malagó

Student: Zubair Muzaffar

Recife

07 November 2019

A Thesis

Experimental Setup to Measure the State of Charge and State of Health of Lead Acid Batteries

By

Zubair Muzaffar (s247017)

Submitted in collaboration with Graduate Engineering faculty of University of Pernambuco to Politecnico di Torino as a partial fulfillment of Master of Science Degree in Automotive Engineering



Luis Arturo Gómez Malagón – Doutor



Marcilio André Felix Feitosa – Doutor



Kénia Carvalho Mendes – Doutor

Politecnico Di Torino

April, 2020

Resumò

Para o amplo sucesso comercial dos veículos eléctricos (VE), é crucial uma compreensão profunda de como as baterias estão a actuar nesta aplicação desafiante. A idéia de colocar células fotovoltaicas na versão mais recente dos carros eléctricos como a energia gerada por eles poderia tomar alguma pressão da bateria principal e alimentar algumas funções eléctricas interiores do carro ou recarregar a bateria. Esta tese foi, portanto, focada no estado de carga da bateria e na estimativa do estado de saúde como uma aplicação de um sistema fotovoltaico fora da rede. Em sistemas fotovoltaicos isolados, a bateria de chumbo-ácido ainda é a tecnologia mais utilizada para o armazenamento de energia e é o componente que tem a menor vida útil do sistema, em torno de 2 a 3 anos, portanto, é um dispositivo que requer atenção especial para que não ocorram, durante sua utilização, situações que reduzem a sua vida útil. Diante dessa criticidade que envolve a bateria, o objetivo desse trabalho foi utilizar a técnica de filtro de Kalman para estimar o estado de carga (SOC) de baterias de chumbo-ácido e embarcar o algoritmo em um microcontrolador Arduino para uso em sistemas fotovoltaicos isolados. O algoritmo requer pouca memória e reduzida capacidade computacional para funcionar, sendo ideal para utilização em um microcontrolador de baixo custo. Para o circuito de monitoramento da bateria, que permite consulta remota aos dados via rede de telefonia celular, foram utilizados um Arduino modelo Mega2560, sensores de corrente e temperatura; e um rádio GSM/GPRS. A bateria utilizada foi uma bateria estacionária ventilada de chumbo-ácido, 12V e capacidade nominal de 200Ah em regime de 10 horas, que equipa um poste solar composto também por módulo fotovoltaico, controlador de carga e luminária. Para os cálculos de parametrização da bateria foi utilizado o software Matlab. Os resultados simulados do estado de carga apresentaram um erro máximo de 2% para a região de 100%SOC a 50%SOC, sendo um valor aceitável uma vez que, apesar do erro, é possível identificar se a bateria está experimentando descargas profundas, isto é, abaixo de 50% da sua capacidade nominal, e/ou recargas ineficientes. Em campo, observou-se que a bateria do poste solar estava sendo descarregada apenas 7,4% da sua capacidade nominal, regime de 10 horas. O circuito de monitoramento remoto apresentou um erro máximo na estimativa do SOC de 1,7%, quando comparado ao método de integração de corrente, na região entre 100%SOC e 92,6%SOC. Por fim, constatou-se a confiabilidade do filtro de Kalman para estimativa do estado de carga de baterias de chumbo-ácido ventiladas bem como a robustez do Arduino para se trabalhar com o algoritmo do filtro.

Palavras-chaves: Sistema fotovoltaico; Bateria de chumbo-ácido; Filtro de Kalman; Estado de carga (SOC).

Abstract

A deep understanding of how batteries are operating in this demanding application is critical for the widespread commercial success of electric vehicles (EVs). The idea to put photovoltaic cells to the latest version of the electric cars as the power generated by them could take some pressure of the main battery pack and power some interior electric functions of the car or recharge the battery. This thesis has therefore been focused on battery state of charge and state of health estimation as an application of an off-grid photovoltaic system. In off-grid photovoltaic systems, the lead-acid battery is still the most used technology for energy storage and is the component that has the shortest life of the system, around 2 to 3 years, so it is a device that requires special attention to ensure that situations do not occur during their use which reduce their lifespan. In view of this battery-critical nature, the objective of this work was to use the Kalman filter technique to estimate the state of charge of lead-acid batteries and to load the algorithm into an Arduino microcontroller for use in off-grid photovoltaic systems. The algorithm requires little memory and reduced computational capacity to function, being ideal for use in a low-cost microcontroller. For the battery monitoring circuit, which allows remote consultation of the data via cellular telephone network, was used an Arduino model Mega2560, current and temperature sensors; and a GSM / GPRS radio. The battery used was a flooded stationary lead-acid battery, 12V and nominal capacity of 200Ah in 10 hours, which equips a solar pole composed also by photovoltaic panel, charge controller and luminaire. The MATLAB software was used for the battery parameterization calculations. The simulated results of state of charge presented a maximum error of 2% for the region of 100% SOC to 50% SOC, being an acceptable value since, despite the error, it is possible to identify if the battery is experiencing deep discharges, this is below 50% of its rated capacity, and / or inefficient recharges. In the field, it was observed that the battery of the solar pole was being discharged only 7.4% of its nominal capacity, regime of 10 hours. The remote monitoring system presented a maximum error in the SOC estimation of 1.7% when compared to the current integration method, in the region between 100% SOC and 92.6% SOC. Finally, it was verified the reliability of the Kalman filter to estimate the state of charge of flooded lead-acid batteries as well as the robustness of the Arduino to work with the filter algorithm.

Keywords: Photovoltaic system; Lead-acid battery; Kalman filtering; State of charge (SOC)

Acknowledgements

I would like to sincerely thank my Supervisor Prof. Andrea Tonoli who gave me guide and support for the course of this work. He carefully reads the manuscript and indicates how to improve the quality of this thesis. I would also render my thanks to Prof. Dr. Luis Arturo Gómez Malagó who asked me to join this work and his time and support he has provided me with for writing this thesis. He always answered the questions patiently and provides insightful advice to cope the problem.

I also acknowledge the rest of the IIT staff for granting us the necessary equipment to perform the task.

I would also like to thank my fellow students Marcelo, Erik, Lorena for their support and encouragement in the areas related to my study and living in Brazil.

Contents

Resumò	3
Abstract	4
1. Introduction	9
2 Theoretical Background	11
2.1 Photovoltaic Systems	11
2.2 Photovoltaic Solar Energy	13
2.3 Solar Cells.....	14
2.4 Photovoltaic Systems in Automotive Industry	15
3 Batteries	17
3.1 Lead-Acid Battery	17
3.2 Types of Lead-Acid Batteries	19
3.3 Characteristics of Lead-Acid Batteries.....	20
4 Charge Controllers	29
4.1 Inverter.....	31
5 State of Charge (SOC).....	31
5.2 Kalman Filter	33
5.3 Algorithm of Kalman Filter	34
5.4 State of the Art	36
6 MATERIALS AND METHODS.....	37
6.1 Material.....	37
6.2 Methods	42
7. Results	44

7.2 Estimation of SOC of the Battery	50
8 Conclusions.....	62
9 References	65
Annex A: Technical specifications of the solar pole components.....	68
Annex B: Technical specification of cycling equipment	70
Annex C: Kalman Filter MATLAB Algorithm.....	71
Annex D: Kalman Filter Arduino Algorithm	72
Annex E: Electronic Circuit Scheme to Monitor the Battery	75

List of Abbreviations

AGM	Absorptive Glass Materials
DOD	Depth of Discharge
GPRS	General Pack Radio Service
GSM	Global System for Mobile
MPPT	Maximum Power Point Tracking
OCV	Open Circuit Voltage
PWM	Pulse Width Modulation
SLI	Start, Lighting, Ignition
SOC	State of Charge
SOH	State of Health
VRLA	Valve Regulated Lead Acid Battery

1. Introduction

Mobility used to be synonymous with equality a decade ago, today's mobility is the norm. With versatility being an electronic device necessity, another falls in - a need for efficient mobile energy storage-a Battery. The battery for an electric vehicle is similar to the fuel tank for a conventional gasoline vehicle. Imagine a vehicle without a fuel level display on the dashboard. Note how difficult it would be for the driver not to have a clear indication of how many miles the car would still travel.

With the popularization of Electric Vehicles and Hybrid-Powered Vehicles, such as buses, forklifts and wheelchairs, there is a increasing need for a Battery Charge Condition predictor, a device or hardware designed to measure the remaining effective power of the battery with only a small number of variables.

Lead acid batteries are common and are used in automobiles for starting the engine and running lights and other electronics. They are also used in certain electric cars, such as golf carts and boats. These are used for security systems, computers, and telephones in addition to mobile apps in battery backup systems.

Battery stacks of lead acid and lithium ion are used in many applications of hybrid electric vehicles (HEV), electric vehicles (EV) and renewable energy storage units for later use. Most traditional cars run on batteries made from lead acid. Lead-acid batteries are fairly cheap, perform well in cold temperatures, and do not put drivers at risk unless they are properly charged. In all these applications, it is necessary to calculate the charging status (SOC) which is the capacity available (for Ah) and expressed as a percentage of the rated capacity. It is also important to measure the state of health of the battery (SOH) which is a measure of the ability of the battery to store and deliver the electrical energy as compared to new battery. Since it is a complex task depending on the type of battery and the application for which it is used. Accurate estimation of SOC helps improving the system performance, lengthen lifespan of the battery and it is one of the main tasks of battery management system. (MARTIN;ADEL)

Lead-acid batteries share in installed batteries is still the highest of all the battery technologies. However, in mobile applications with the replacement of the combustion engine by electric motors, the attention paid to lead-acid batteries will abate. If the costs stay competitive with respect to lithium-ion batteries, stationary installations lead-acid batteries will remain attractive. A typical stationary application is Photovoltaics system (PV), in which the batteries are float-charged until their stored energy is required. (JAVIER, 2014)

The system developed in this work presented a total cost of R\$550.00. Despite the low cost, the system is capable of to estimate in real time the state of charge of the batteries monitored by him, besides to allow expansion for current and voltage monitoring of up to 8 batteries simultaneously, plus the ambient temperature. For this expansion, an extra cost average of R\$50.00 would be necessary. In addition, the system is equipped with a GSM/GPRS module that allows remote monitoring via the Internet or via GSM mobile phone network, dispensing with the technician's frequent visit to data collection and subsequent analysis.

Having as justification the questions presented here and as motivation the great growth potential of photovoltaic solar energy in Brazil, according to the data presented, this work has the objectives:

1) General Objectives

Use the Kalman filter technique to estimate the state of charge of 12V lead-acid vented stationary batteries and ship the algorithm in a low-cost microcontroller for use in isolated photovoltaic systems.

- i) Structure the electronic circuit for remote monitoring of the state of charge of lead-acid ventilated batteries;
- ii) Perform the modeling of lead-acid batteries ventilated for use in computer simulations;
- iii) To evaluate the behavior of a lead-acid battery in the field, installed in a solar pole, through the instrumentation of this photovoltaic solar system.

To verify the operation and efficiency of the device, all data in this research was created from this prototype of engineering. The results show that this setup is a promising design for a cost-effective, high efficiency.

2) Thesis Structure and Methodology

Thesis is divided into two parts- theoretical and practical, where secondary research, qualitative and quantitative methods are used.

To present the relevant data by the end of the work, the thesis will comprise of a comprehensive review of books, journals, scientific articles, surveys and various companies' reports published online. With the help of the secondary data analysis, I will research existing theoretical information to better understand the concept and be able to give recommendations on how to apply it in practice.

Briefly, quantitative research refers to the explanation of a concept by means of numerical data, graphs and charts, different setup figures while qualitative is based on people's subjective thinking, their opinions and perceptions of certain issues.

In the first part, an off-grid photovoltaic system is installed in the lab. The setup consists of solar panels which are connected with batteries and microcontrollers are connected respectively along with other components such as current, voltage, temperature sensors and inverter. The batteries charging and discharging data is recorded at different time intervals of the day.

In the second place, the data collected is analyzed through experimental method in order to estimate the state of charge (SOC) of the battery. It is supported with theoretical background of each component used to install the system and qualitative approach to select the components.

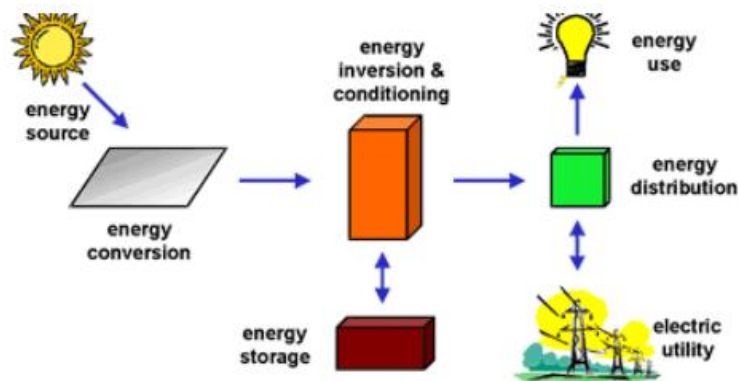
2 Theoretical Background

2.1 Photovoltaic Systems

Simply put, PV systems, like any other electrical generating system, are distinct from the devices used for traditional electromechanical generating systems. The working and interfacing rules with other electrical systems, however, remain the same and are controlled by a well-established set of electrical codes and standards. Although, when exposed to sunlight, a PV array produces power. To properly conduct, control, convert, distribute and store the energy produced by array, several other components.

The particular components required for the system, based on the functional and operational specifications, may include a DC-AC power inverter, battery bank, system and battery controller, auxiliary power sources and sometimes the electrical load (appliances) specified. Furthermore, a range of system balance (BOS) hardware, including cable, overcurrent, surge protection and disconnect systems, and other energy processing equipment. **Figure 2.1** shows a basic photovoltaic system diagram and the component relationship. (JAVIER, 2014)

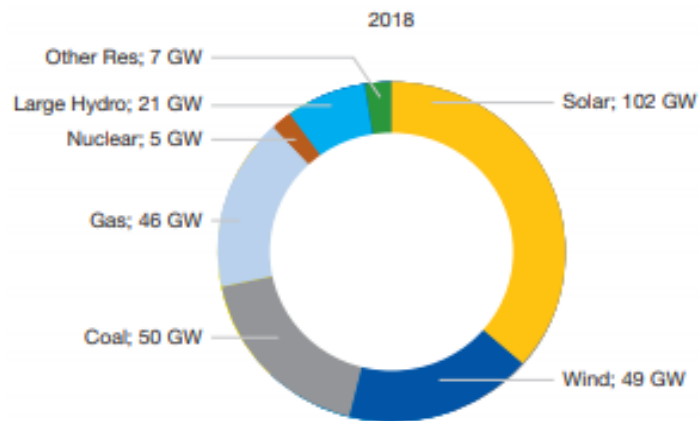
(Fig 2.1 – Major Photovoltaic System Components)



Source: (JAVIER, 2014)

A recent report by Solar Power Europe and Global Solar Council, in 2018 solar broke the 100 GW threshold of annual installations, and it will be recalled as the year solar in total reached a cumulative operational capacity of over 500 GW or 0.5 TW. The net power generating capacity added in 2018 by main technology is illustrated in (**Figure 2.2-** European Council of Solar Energy). (Walburga & Micheal, 2019)

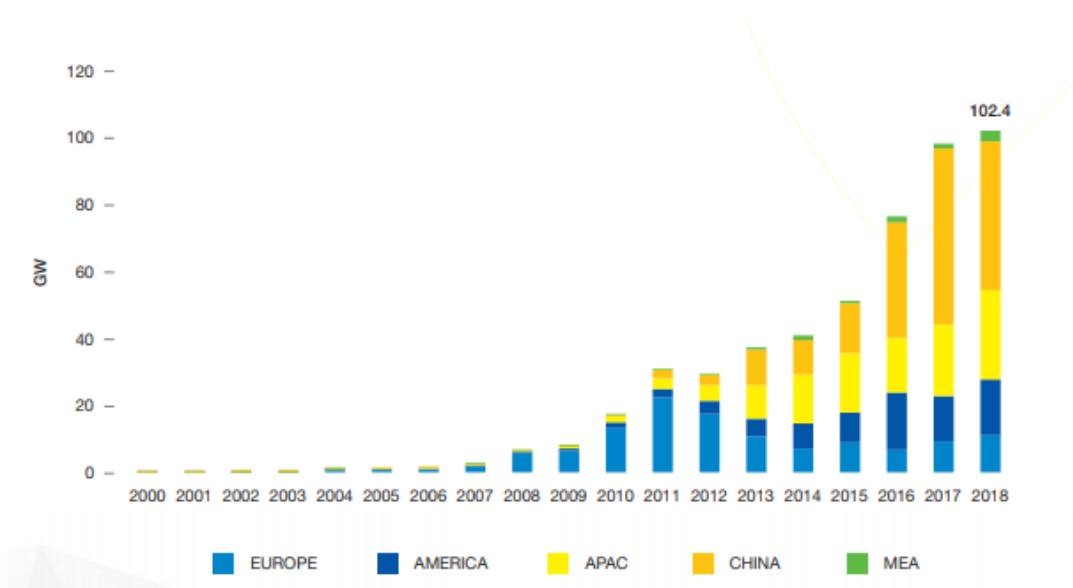
(Fig.2.2-Added Power Generating Capacity in 2018)



Source: (Walburga & Micheal, 2019)

A total of 102.4 GW went on the grid around the world in 2018 (Fig.2.2). That's still 4% more than the 98.5 GW installed in 2017 but compares to two years with very high growth rates – around 30% in 2017 and 50% in 2016 shown in (Figure 2.3)

(Fig2.3- Evolution of Global Annual PV Installed Capacity 2000-2018)



Source: (Walburga & Micheal, 2019)

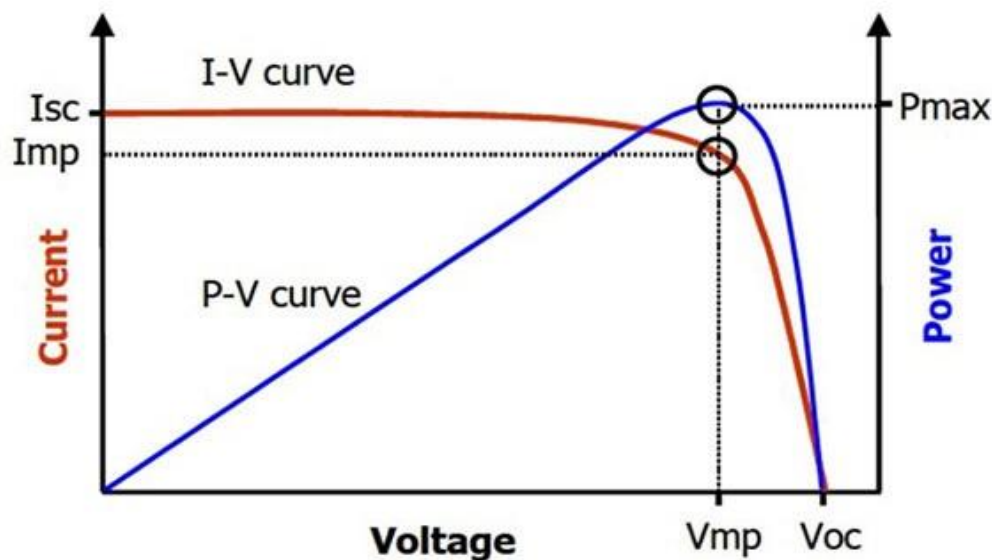
According to the Synthesis Report of the 2018 National Energy Balance (Base Year 2017) of the Energy Research Company - EPE, the electric power generation by photovoltaic solar source was 359.1 GWh, which represented a participation of 0.4% in the total power generation considering all sources. Compared to the generation of energy by solar photovoltaic source in 2016, there was a significant increase of 875.6%. Much of this increase is due to recent regulatory actions that made it possible to offset the surplus energy produced by smaller systems. The states that lead the national ranking in distributed generation are Minas Gerais, with an installed capacity of 109.5 MW, Rio Grande do Sul, with an installed capacity of 78.8 MW and São Paulo, with an

installed capacity of 61.2 MW. Together, these three states account for approximately 50% of the total installed power in Brazil of distributed generation. (EPE BRASIL, 2018)

The I-V characteristic curve is one of the main parameters of a module photovoltaic. The curve consists of pairs of voltage and current data that describe the current response of the photovoltaic module when subjected to a variable voltage (PINHO; GALDINO, 2014).

Figure 2.4 shows the I-V characteristic curve of a solar cell of silicon, where I_{sc} is the electrical short-circuit current, you are the open circuit voltage, P_{MP} is the maximum or peak power and I_{MP} and V_{MP} are the maximum current and voltage power, respectively.

(Fig.2.4 I-V characteristic curve of a silicon solar cell. Electrical current as a function of the power difference applied to a silicon solar cell.)



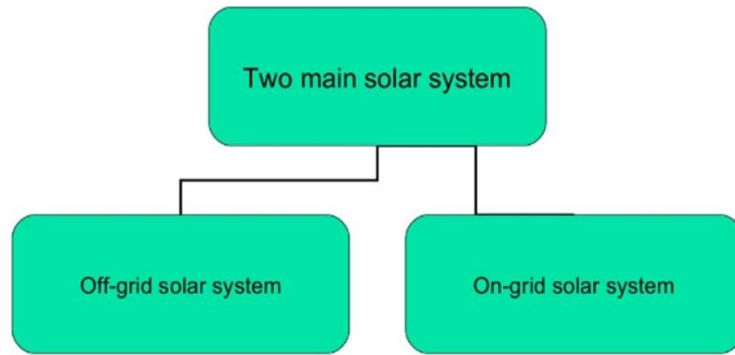
2.2 Photovoltaic Solar Energy

Photovoltaic solar energy is electrical power generation measured in watts (W) or kilowatts (kW) using direct electrical current (DC) generated by semiconductors when illuminated by photons. The solar cell, the name given to the photovoltaic element, converts light energy into electrical energy while light illuminates it. When there is no light generation ends.

Photovoltaic solar power equipment generates electricity without producing greenhouse gas or other gas emissions and works in a silent manner. Solar photovoltaic systems main disadvantage is the high value of the initial investment. (JAVIER, 2014)

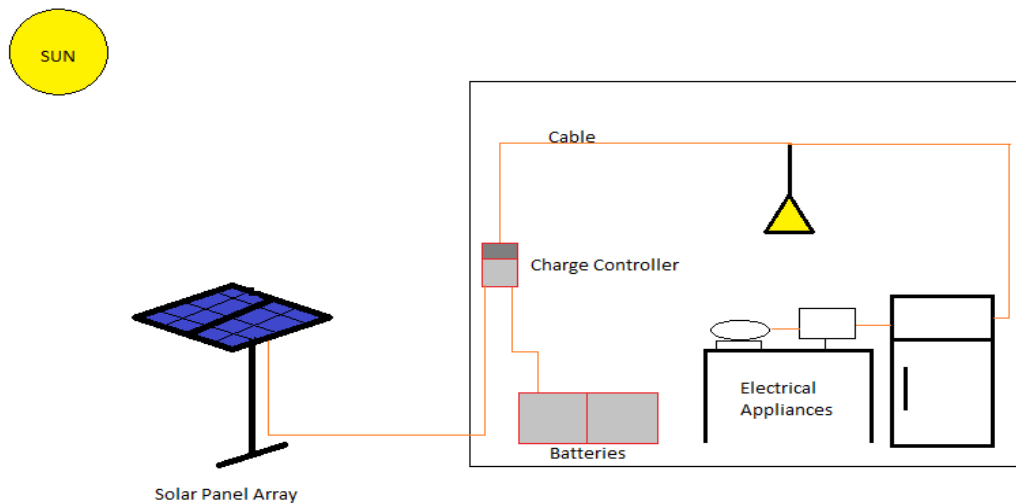
There are two main categories of photovoltaic systems:

- Grid Connected
- Isolated (Off-grid)



Isolated systems can be purely photovoltaic, operating only from a photovoltaic source; or hybrid, combining photovoltaic generation with one or more sources of energy (for example, diesel generator or wind turbine). Both of them require some type of storage. If you want to use electrical appliances during periods when there is no photovoltaic generation, storage can be in batteries. (PINHO & GALDINO, 2014)

A scheme of the isolated photovoltaic system is shown in [Figure 2.5](#).

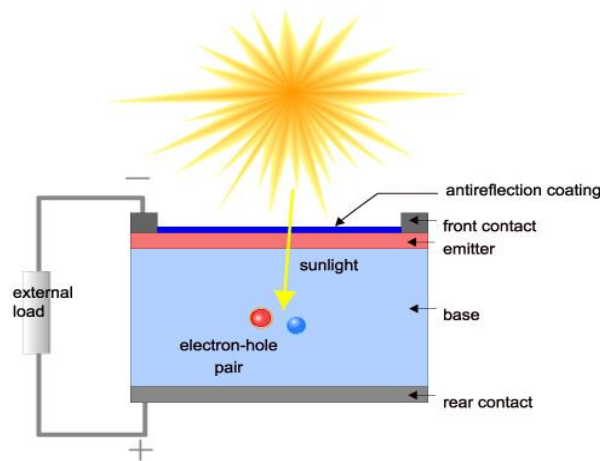


Source: Writer

2.3 Solar Cells

Solar cells are generally made of silicon, the same material that is used for transistors and integrated circuits. The silicon is treated or "doped" to release electrons when light strikes so that an electrical current is produced. There are three basic solar cell types. Monocrystalline cells are cut from a silicon ingot from a single large silicon crystal, while polycrystalline cells are cut from an ingot consisting of many smaller crystals. The third type is the solar cell that is amorphous or thin film. (JAVIER, 2014)

(Fig2.6 – Cross -Section of Solar Cell)



a) Amorphous Solar Cells

Amorphous technology is most commonly seen in small solar panels, such as calculators or garden lamps, despite the increasing use of amorphous panels in larger applications. These are made by putting a thin silicon film on a surface of other material like metal. The panel is shaped as one piece, and not as visible as in other forms are the individual cells. The performance of amorphous solar panels is not as high as those produced from individual solar cells, although in recent years this has increased to the point where they can be seen as a practical alternative to crystalline cell panels. Their great advantage is that they generate relatively low power cost per W. However, this can be offset by their lower power density; for the same power output, more panels are needed, and more space is therefore taken up.

b) Crystalline Solar Cells

To produce solar panels, crystalline solar cells are wired in series. Since each cell produces a voltage between 0.5 and 0.6 Volts, an open circuit voltage of about 20 Volts requires 36 cells. This is enough for most conditions to charge a 12 Volt battery.

While the theoretical efficiency of mono-crystalline cells is slightly higher than that of poly-crystalline cells, there is little practical quality difference. Generally, crystalline cells have a longer life than the amorphous form.

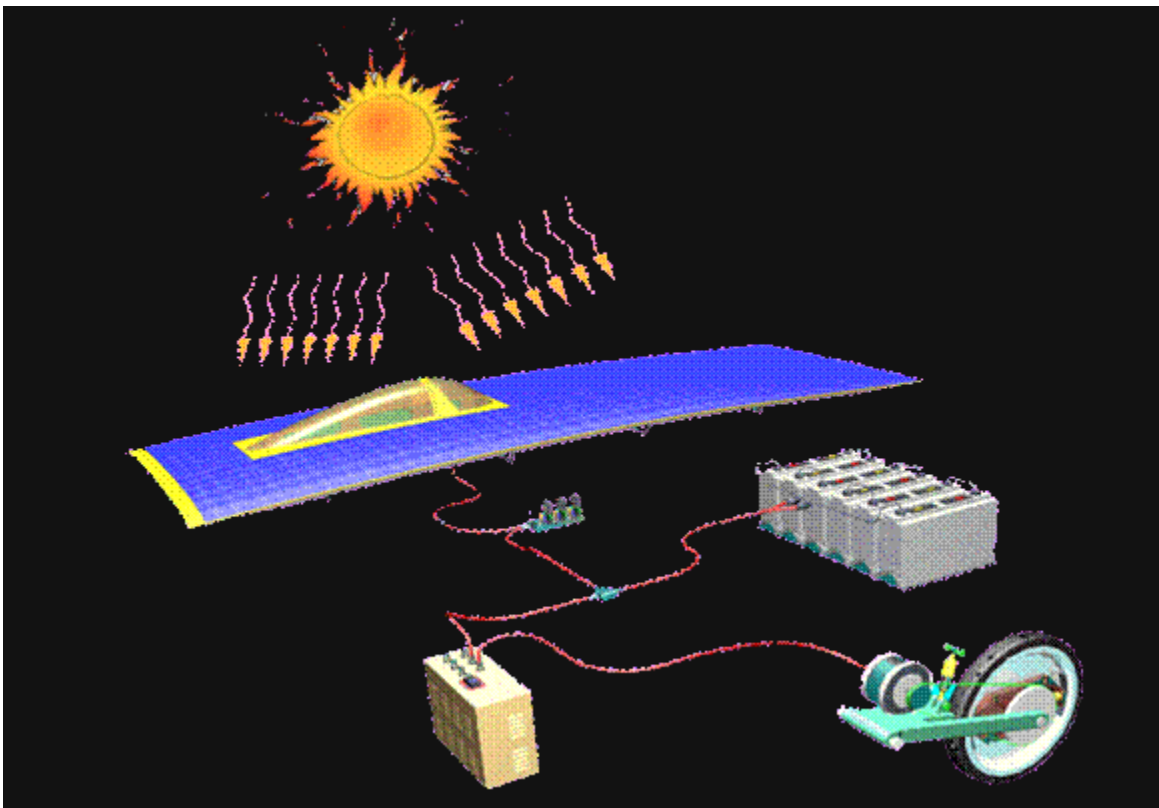
2.4 Photovoltaic Systems in Automotive Industry

The first solar car that had been invented was a tiny 15-inch vehicle made by General Motors William G. Cobb. Called the Sun mobile, on 31 August 1955 Cobb displayed the first solar car at the Chicago Powerama convention. The solar car consisted of 12 photovoltaic selenium cells and a small Pooley electric motor turning a pulley which turned the rear wheel shaft rotating in turn.



There are significant differences between use of solar energy and all other types of powering the cars. Unlike solar-powered houses, solar cars harvest energy from the sun, turning it into electricity. That electricity then fuels the car's motor-driven battery. Many solar cars channel the power directly to an electric motor, rather than using a battery. This can be achieved in solar cars through Photovoltaic Cells (PVC). (CRISTEN CONGER)

2.4.1 Energy Flow Scheme in Solar Cars



Source: Solar Cars Seminar

3 Batteries

3.1 Lead-Acid Battery

Battery is a chemical device for electricity storage (DELL; RAND, 2011) that converts the chemical energy contained in its active material directly into electrical energy through electrochemical oxidization reactions (redox). The battery device can be classified in several ways depending on, for example, the chemical elements in the active material of the positive and negative electrodes; and whether or not it can be recharged (LINDEN, 2011).

The battery is formed by basic electrochemical units, called cells, which directly convert chemical energy into electrical energy. The cell consists of a set formed by positive and negative electrodes, separators, electrolyte, case and terminal (LINDEN, 2011). The positive electrode or cathode accepts electrons from the external circuit and reduces during electrochemical reactions. The electrode or anode provides electrons to the external circuit and is oxidized during the electrochemical reactions. The electrolyte, the ionic conductor, is the means of transfer of load through ions, inside the cell between the anode and the cathode. Typically, the electrolyte is a liquid, such as water or other solvent, with dissolved salt, acid or alkali to make ionic conductivity possible (LINDEN, 2011).

The lead-acid battery uses lead dioxide (PbO₂) as the active material in the positive electrode and metallic lead (Pb), with a high porous structure area surface, as negative active material. The electrolyte is a solution of sulfuric acid (LINDEN, 2011). **Figure 3.1** summarizes the chemical reactions that take place in the electrodes and presents the general equation of the process.

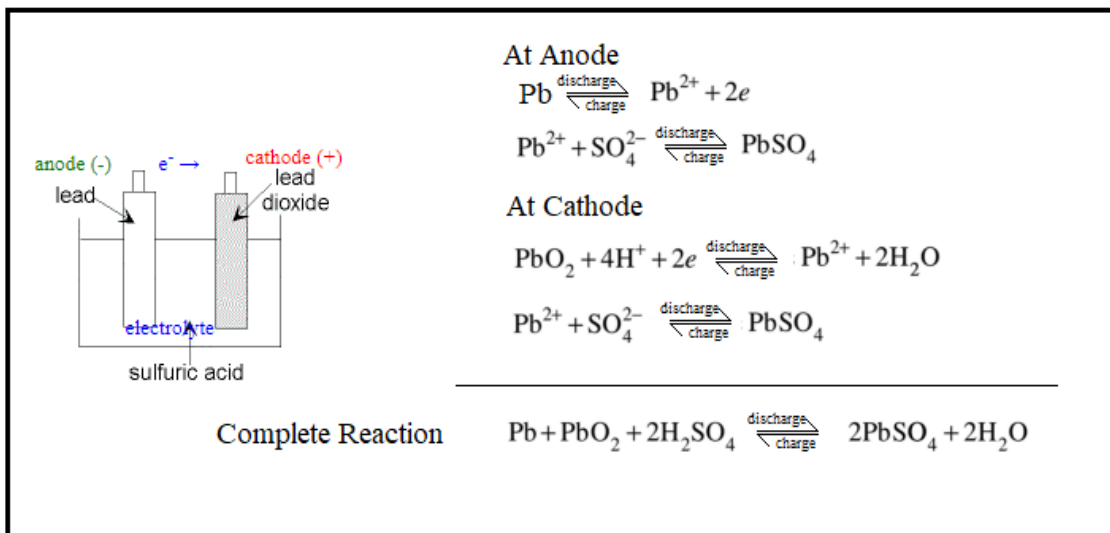


Fig. Chemical Reaction of a Lead-Acid Battery

Source: Writer

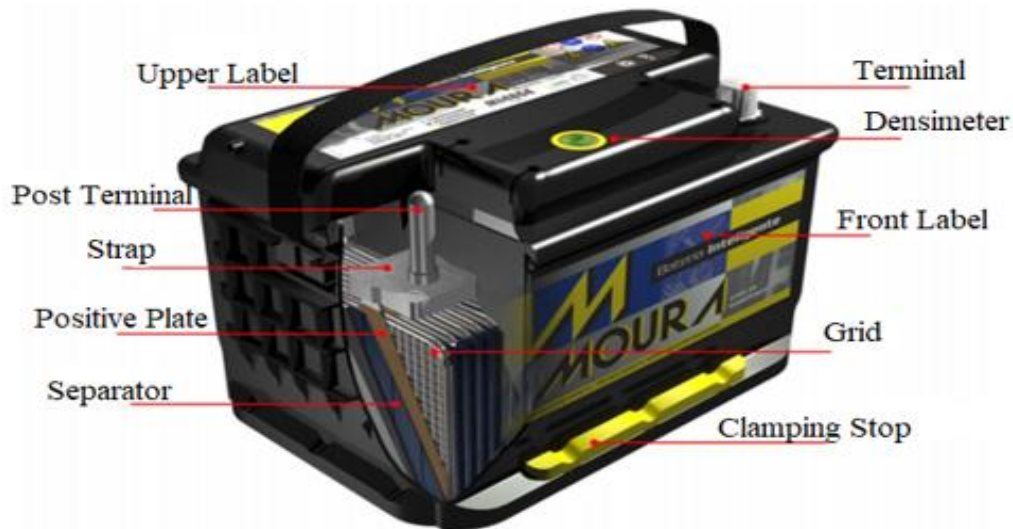
In **Figure 3.1** it is observed that, during the discharge, the chemical reaction happens from left to right. Conversely, during the recharge, the reaction happens in the opposite direction. During the discharge, both electrodes are chemically matched and transformed into lead sulphate (PbSO₄).

The battery consists of one or more connected electrochemical cells electrically in appropriate arrangement, or in series or in parallel, so as to provide the required voltage and current (LINDEN, 2011). The association of parallel cells provides the increase of the current provided by the set; the serial cell association increases the nominal voltage of the battery.

Figure 3.1 presents a cutting view of a lead-acid battery that shows some of its main internal and external components, namely, 1) the grid, component responsible for conducting electric current as well as for sustaining the active material of the positive and negative electrodes; 2) positive and negative plates, formed by joining the positive active material (positive mass) and the positive grid; and the union of the negative active material (negative mass) and the negative grid, respectively; 3) separator, responsible for the electrical isolation between the plates negative and positive allowing ionic conduction through the electrolyte; 4) strap, which connects the plates of the same electrode in parallel, that is, positive plates of the same electrode cell connected to each other and negative plates of the same cell also connected between them. The strap is also the device that connects adjacent cells in series.

The end post, named after the straps on the ends of the assembly, is welded with the terminal to form the positive and negative poles of the battery. The terminal pole connects the inside of the battery to its outside, making it possible to connect the loads that are powered by the accumulator through the terminal block. The external items as labels, fixing stops and densimeter vary with the manufacturer and has functions of product identification, fixing and storage; and conditions of battery use, respectively.

(Fig.3.2 Sectional view of Battery)



Source: Moura, 2017

3.2 Types of Lead-Acid Batteries

Lead-acid batteries can be classified according to their intended application, as well as whether or not they require maintenance. Batteries are classified according to the application as (PAVLOV, 2017):

- a) SLI Batteries, from Start, Lighting, Ignition; used in cars. Its main function is to put the internal combustion engine in operation through fast high current discharge.
- b) Stationary batteries, commonly used as energy sources backup, i.e. provide and store electrical power for use, on demand, in telecommunications systems, power plants, computer systems etc. Batteries for photovoltaic systems isolated are in that category.
- c) Traction batteries are industrial batteries for traction vehicles of handling in indoor environments such as forklifts, cars electrical, mining equipment etc.
- d) Special-purpose batteries for use in aircraft, submarines and special military equipment.

Regarding maintenance, lead-acid batteries are classified as (PAVLOV, 2017):

- a) Flooded, English flooded batteries, with high antimony content in the alloy of the bars. These batteries require regular maintenance. Maintenance mostly consists of adding demineralized water to the battery cells.
- b) Maintenance-free or ventilated batteries, with positive lead-calcium tin alloy plates and, for the negative plate, lead-calcium alloy grids. This has been the type of battery that has been most used in isolated photovoltaic systems in Brazil (PINHO; GALDINO, 2014).
- c) Valve Regulated Lead-Acid Battery (VRLA). This type of battery, unlike the others that have the electrolyte in liquid state, has the electrolyte absorbed in the fiberglass blanket separator, the Absorbent Glass Mat (AGM); or has the electrolyte in gel form, also known as gel batteries. Both types are equipped with exhaust valves which, when the pressure rises, the valve opens in a predetermined value, releasing the gases. VRLA technology reduces the emission of gases by up to 95% when compared with batteries of liquid electrolyte (LINDEN, 2011).

A lead-acid battery of VRLA technology, according to authors as Pine and Galdino (2014) and Pavlov (2017); and manufacturers as Enersys (2017), Sacred-Sun (2018) and Moura (2018), must respect the temperature limit of operation between 20°C and 30°C. Also, according to the manufacturers, a VRLA battery has its service life reduced by half when operated at a temperature of 10°C above the recommended operating temperature of 25°C. Hariprakash et al. (2008) concluded that the VRLA battery is the most suitable for use in isolated photovoltaic systems for lighting.

For our case, it was observed that the scenario in which the ventilated battery object of this study was inserted had adverse temperature characteristics to the technology VRLA. This reinforces the relevance of this work to implement the monitoring system for stationary lead acid batteries ventilated in view of the lack of published works with this scope specific.

Data from the company Acumuladores Moura S/A indicate that, in Brazil, stationary VRLA batteries are mainly used in back-up systems of energy for the telecommunications and data center market. Virtually 100% of VRLA stationary batteries are imported products. In 2016, around 140

thousand 12V VRLA stationary batteries were imported for use in applications quoted. Generally, the places where VRLA stationary batteries are installed are equipped with air conditioning systems for temperature control of the environment, configuration that, for an isolated photovoltaic system, deserves a study feasibility and analysis of the impact of air conditioning load on consumption total of the main loads of the facility.

3.3 Characteristics of Lead-Acid Batteries

The popularity of lead-acid batteries is partly due to their high open circuit voltage (approximately 2.1V per cell) among other factors positive as low cost, versatility and excellent reversibility of the electrochemical pair (DELL; RAND, 2001). Besides being able to offer high power, lead-acid batteries are reliable and easy to produce. The resources for its manufacture are practically unlimited. Around 95% of the materials used in a lead-acid battery are recyclable. Finally, a lead-acid battery can keep your energy stored for a long period of time (PAVLOV,2017).

3.3.1 Capacity

The amount of charge stored in a battery is defined as Capacity, expressed in ampere-hour (Ah), represented mathematically as the integral of the discharge current in time, as follows

$$Capacidade (Ah) = \int I dt$$

where I is the battery discharge current in ampere; and t the duration of the discharge in hours (DELL; RAND, 2001). Cutoff voltage is defined as the value of the voltage at which the battery discharge is interrupted (PINHO; GALDINO, 2014).

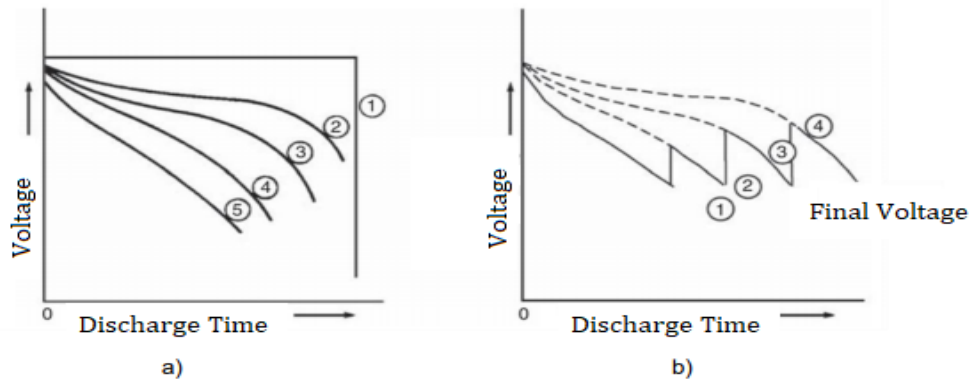
One of the main parameters of the battery is the Nominal Capacity, defined as a conservative estimate by the manufacturer, of the total number of ampere hours that can be taken from a new cell or battery, for the specified values (according to certain standards or norms, or by the manufacturer itself) of discharge current, temperature and cut-off voltage (PINHO; GALDINO, 2014). In Brazil, from in accordance with Inmetro Ordinance No. 004 (2011) establishing the criteria for the Conformity Assessment Program for Energy Systems and Equipment photovoltaic, the manufacturer of lead-acid batteries for photovoltaic systems shall specify the nominal capacity for a 10-hour scheme at a 25°C temperature and 10.5 volts cut-off voltage.

A widely used concept is the charging/discharge rate concept which indicates the charging or discharging current used to charge or discharge the battery, respectively. For example, a battery that has a C10 of 200Ah, means that this battery provides in 10 hours (discharge rate C10), a total capacity of 200Ah, when discharged with a constant current of 20A.

The relationship between the current with which the battery is discharged (discharge rate) and the time to reach the cut-off voltage is established as, the higher the discharge current, the shorter the time to reach the cut-off voltage, and therefore the lower battery capacity (LINDEN, 2011 and PINHO; GALDINO, 2014). **Figure 3.3a**) presents this relationship graphically through discharge curves with distinct currents. With extremely low discharge current (Curve 2) the discharge approaches the theoretical voltage and capacity (Curve 1). As the current increases (Curve 3 to 5), the voltage at the discharge decreases, the slope of the curve if shows more pronounced, and

available capacity in ampere-hours is reduced. At **Figure 3.3b**) it is observed that, if the battery reaches a certain voltage, by example, the cutting voltage, when discharged with a given current and the discharge continue with a lower current, its voltage will rise and a capacity will be obtained until the cutting voltage is reached again.

(Fig.3.3 Characteristic of battery voltage during discharges with different currents)



Source: Linden, 2011.

3.3.2 Energy Efficiency

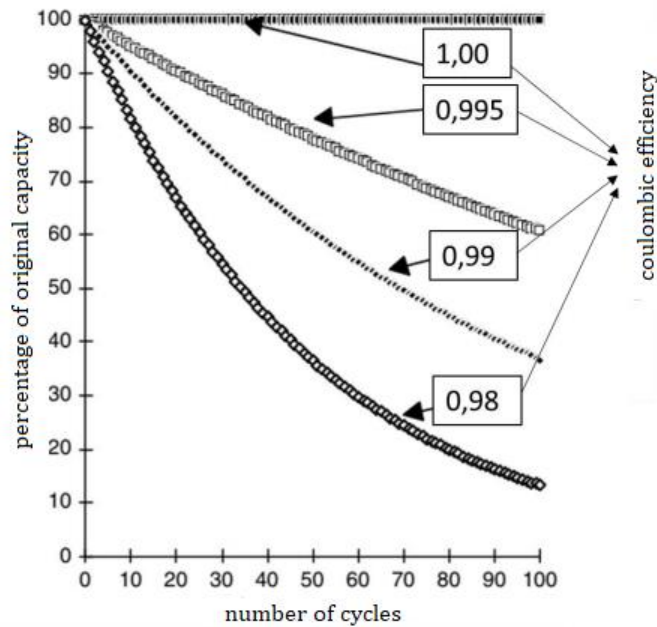
The amount of power taken from a battery, measured in watt-hours, is always less than the power used to recharge the battery. The ratio of energy withdrawn (discharge) to energy input (recharge) is defined as the energy efficiency of charging and discharging the battery (DELL; RAND, 2001) and is made up of the coulombic efficiency and voltage efficiency, defined below (PINHO; GALDINO, 2014):

- Coulombic or ampere-hour efficiency (Ah): is the ratio between the amount of electrical charge (Ah) that a cell provides at discharge and the amount of electrical charge needed at recharging to restore the initial state of charge, calculated by the ratio between the integrals of the current over the time of discharge and charge. A lead-acid battery has a typical 95% coulombic efficiency.
- Voltage or voltage efficiency (V): is the ratio of the average voltage at the discharge of a cell or battery to the average voltage at the load necessary to restore the initial capacity. In a typical photovoltaic system, the 12V lead-acid battery is charged at an average voltage of 13.8V and discharged at an average voltage of 12.5V, thus the voltaic efficiency approaches 90.5%.
- Energy efficiency or watt-hour efficiency (Wh): also known as overall efficiency, it is the product of the coulombic and voltaic efficiencies. According to the above values, for a lead-acid battery, it is established that the energy efficiency is approximately 86%.

For many user's energy efficiency is irrelevant due to the low cost of electricity and why other factors are more relevant in choosing a battery. In isolated photovoltaic systems where the battery should be the most efficient possible to avoid wasting energy generated by the solar panel array energy efficiency becomes a parameter of relevance (DELL; RAND, 2001). For the case of

coulombic efficiency, specifically, keeping its value the highest possible is a challenge for the battery design mainly when intended to applications involving many loading and unloading cycles, such as a system photovoltaic, because every cycle there is a loss of available battery capacity, as can be seen in Figure 3.4 (HUGGINS, 2009). In Figure 3.4 it can be seen that even efficiencies close to the unit can be important consequences every cycle. For example, a loss of 0.5% of capacity available per cycle provides an available capacity of 78% of the capacity original after 50 loading and unloading cycles. After 100 cycles, only 61% of original capacity remains. This situation worsens if the coulombic efficiency is minor.

(Fig.3.4 - Influence of the coulombic efficiency on the available capacity during loading and unloading cycles.)



Source: Huggins (2009)

3.3.3 Specific Energy

Specific Energy is the energy stored per unit mass, expressed in watt-hours per kilogram of mass (Wh.kg⁻¹).

The lead-acid battery shows the lowest specific energy among the major battery technologies, in order from 30 to 40Wh.kg⁻¹ while a lithium-based battery has between 80 and 200 Wh.kg⁻¹ of specific energy. This is due to the high atomic mass of lead which results in an excessive total weight of the battery, configuring the biggest disadvantage of the batteries of lead-acid (PAVLOV, 2017 and DELL; RAND, 2001).

(Table 3. Main features of various battery technologies)

System	Voltage (V)	Specific Energy (Wh.kg ⁻¹)	Energy Density (Wh.L ⁻¹)	Power Density (W. kg ⁻¹)	Specific Energy of the Battery (100%SOC) (Wh. kg ⁻¹)
Lead-acid	2,1	30-40	60-75	180	20-35
Nickel-Cadmium (Ni-Cd)	1,2	40-60	50-150	150	40-60
Nickle-Metal hydrate (Ni-MH)	1,2	30-80	140-300	250-1000	40-70
Lithium-Ions LiCoO ₂	3,6	160	270	1800	
Lithium Polymer	3,7	130-200	300	3000	
Lithium- Ions LiFePO ₄	3,25	80-120	170	1400	

Source: Pavlov (2017)

3.3.4 Operating Voltage

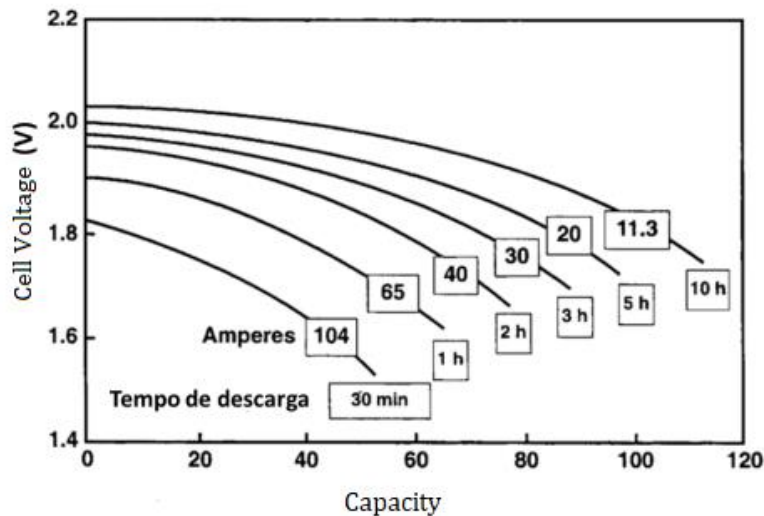
The nominal voltage of a lead-acid cell is 2 V. The voltage of open circuit is a direct function of electrolyte concentration. The lead acid cell operates with a sulphuric acid solution (H₂SO₄) with a concentration of up to 1.28g.cm⁻³ at 25°C.

For a moderate discharge, the cut-off voltage is 1.75V per cell, while for high discharge rates at low temperatures, the cut-off voltage can be as low as 1V per cell (LINDEN, 2011).

As shown in Item 2.2.2, the higher the discharge current of a battery, the shorter the time to reach the cut-off voltage, and therefore the lower the battery capacity (LINDEN, 2011; DELL; RAND, 2001 and PINHO; GALDINO, 2014). **Figure 3.5** shows this typical ratio for a lead acid battery. In the 104A current curve, it is observed that the battery reaches a voltage per cell of approximately 1.5V in 30 minutes, resulting in a capacity of 52Ah (104A x 0.5h), observed in the abscissa axis. With a current of 65A, the battery reaches a voltage per cell of 1.6V in 1-hour time, resulting in a capacity of 65Ah (65A x 1h), i.e. a capacity greater than the first case.

Finally, with a current of 11.3A, the battery takes 10 hours to reach a voltage per cell of approximately 1.75V, resulting in a capacity of 113Ah.

(Fig.3.5 Discharge curves of a lead-acid battery with nominal capacity in 5h, C5, 100Ah.)



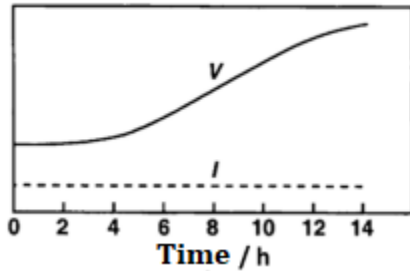
According to the literature, there are several methods for charging a lead-acid battery. There are four basic charging methods, namely constant current method, constant voltage method, constant current and constant voltage method and finally taper method, detailed below and graphically illustrated in [Figure 3.6](#) (DELL; RAND, 2001):

- a. constant current charging consists of using a constant current during the entire loading process. The value of the current must be chosen carefully since if the current is too low, the charging process is very slow if the current is too high, there will be excessive gasification. Ideally, a high current is employed during the first half of the loading process, then by a smaller current in the subsequent stages (load with two stages). According to Linden (2011), this process is not largely used for lead-acid battery charging.
- b. constant voltage load: when under constant voltage load, the value of the current supplied is determined by the difference in voltage between the charger and the battery. The current starts at a high value and decreases approximately exponentially as the load proceeds. This method of loading is employed in a use of the battery known as fluctuation which is characterized by keep the battery fully charged through continuous application of a specified voltage, known as fluctuation stress. A voltage should be carefully limited to avoid a current which would result in an overload and increase in the rate of loss of water (LINDEN, 2011). The fluctuation regime is mainly applied on stationary batteries. The fluctuation voltage for a lead-acid is between 2.17 and 2.25V.
- c. Constant current and constant voltage charging: at this charging rate the current remains constant until the battery reaches a predetermined voltage value where gasification probably starts. At this point, the voltage remains constant and the current decreases exponentially, following the example of the constant voltage charging method.

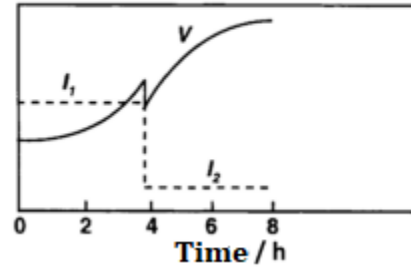
- d. Taper load: the current starts at a high value and decreases as the battery voltage increases. Generally, the end of the charge is controlled by a fixed voltage. Domestic chargers for use in automotive batteries generally use this type of charge.

(Fig.3.6 Charging methods a) constant current charging - single stage; b) constant current charging - two stages; c) constant voltage charging; d) taper charging - single stage; e) constant current and constant voltage charging.)

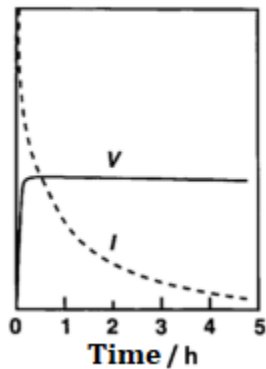
(a) Constant Current: one step



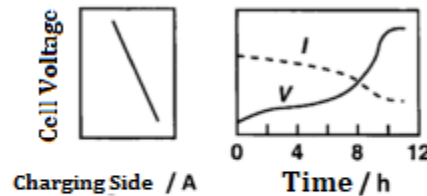
(b) Constant Current: Two Steps



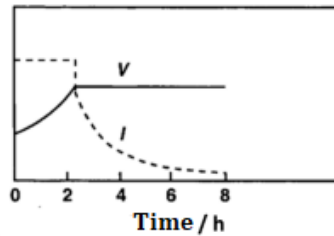
(c) Constant Voltage



(d) Taper: Single Step



(e) Constant Voltage and Current



3.3.5 Operating Temperature

The temperature at which the battery is discharged has a pronounced effect on its capacity and voltage characteristics (LINDEN & REDDY, 2011). According to the standard document ABNT NBR 14199 (2018), for a lead-acid battery, the capacity value obtained at any temperature must be corrected to the reference temperature of 25°C according to

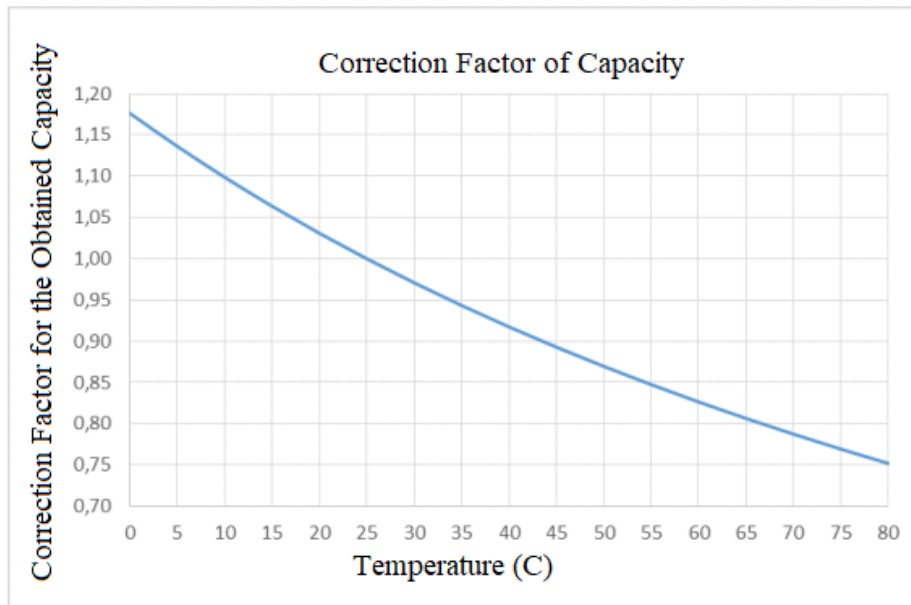
$$C_{25} = \frac{C_T}{1 + \lambda(T - 25)} = kC_T;$$

Where;

- C_{25} : is the corrected capacity for 25°C;
- C_T : is the capacity at temperature T;
- λ : is the temperature coefficient for the capacity (0.006 for regimes 1h and 0.01 for regimes ≤ 1 h);
- T: is the temperature of the electrolyte or battery, expressed in degrees Celsius (°C).
- k is the capacity correction factor at temperature T.

Figure shows, for a commercial lead-acid battery, the k-factor curve for capacity correction obtained by temperature T.

(Fig.3.7- Correction Factor of Capacity)



Source: Moura, 2019

3.3.6 Cyclic Life

Cyclic life is defined as the number of times the battery can be effectively recharged before its stored capacity is below 80% of its maximum capacity (HADDAD; SHAHAT; KALAANI, 2015). High cyclic life is a desired feature for applications such as isolated photovoltaic systems, where the battery experiences daily charge cycles and download (PINHO; GALDINO, 2014). Applications involving many cycles require the battery to be built in such a way that it has an extremely low loss of capacity per cycle, i.e. have a coulombic efficiency as high as possible (HUGGINS, 2009).

The cyclic life of a battery is critically dependent on the cyclic regime to which she is submitted, that is, her cycling history. Cycles with discharge Depth of Discharge (DOD) depth, reduce life battery cyclic due to the appearance of sulphation, a phenomenon that typically occurs during battery discharge and is characterized by the lead (PbSO_4) in the electrode plates. Although it is a natural product of process of energy conversion in the battery, lead sulphate crystals can become larger and larger if the battery remains flat for a long time, making it difficult to convert lead sulphate back into active material, which results in loss of battery capacity and cyclic life (PINHO; GALDINO, 2014). Still, batteries are usually designed to withstand a high number of cycles (>300 cycles) with depth of discharge around 25% of your nominal capacity (DELL; RAND, 2001).

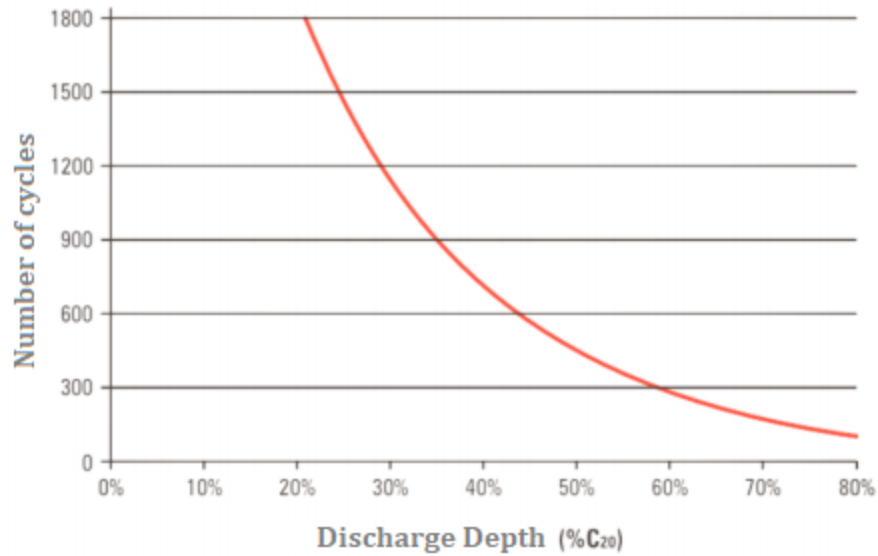
In addition to the depth of discharge, when the battery's operating temperature increases, its capacity rapidly deteriorates (PINHO; GALDINO, 2014). **Figure 3.8** shows the cycling resistance behavior of a lead-acid battery as a function of the depth of discharge to which it is subjected. **Figure 3.9** shows typical curves of the effect of discharge depth and temperature on battery life.

In Brazil, according to Inmetro Ordinance No. 004 (2011) which establishes the criteria for the Conformity Assessment Program for systems and equipment for photovoltaic energy, for lead-acid batteries, shallow cycle represents a depth of discharge (DOD) of 25% of the nominal capacity (C10) of the battery, while in deep cycle, the battery suffers a depth of discharge of 75% of its nominal capacity (C10). To comply with the ordinance, the lead-acid battery should have a capacity above 80% of its C10 nominal after at least 150 cycles divided into 50 deep cycles (Phase A) followed by 100 shallow cycles (Phase B). During the cycles, the battery must be at environment with a temperature of 40°C . The capacity test is performed at a temperature of 25°C . Generally, the final amount of cycles that the battery supports will be reported by the manufacturer in multiples of 150, i.e. 150 cycles, 300 cycles, 450 cycles, etc.

In practice, in isolated photovoltaic systems, deep cycles occur when recharging the battery is not sufficient to replenish the amount of charge taken to power the devices throughout the day. Therefore, the state of charge of the battery is slightly reduced with each daily cycle and, if it happens for a period of several days, the result will be a deep cycle (PINHO; GALDINO, 2014). During normal battery operation, the maximum discharge depth should be limited. For photovoltaic system batteries, the maximum discharge depth should be 50% of the nominal capacity in a 10-hour regime (ZHAO, 2013), i.e. a battery of nominal capacity of 200Ah should not exceed a discharge of 100Ah during its use.

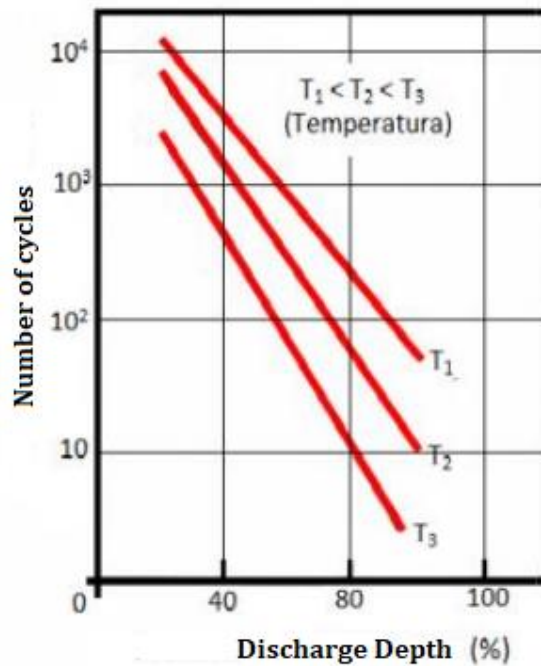
Operational experiences reveal that the lifetime of batteries used in photovoltaic systems is generally unsatisfactory compared to the lifetime in other traditional applications. Data from battery manufacturer Acumuladores Moura S/A (2017) show that in isolated solar systems, batteries have an average life of 2 to 3 years.

(Fig.3.8 Number of cycles depending on the depth of discharge of a lead-acid battery)



Source: Moura,2016

(Fig.3.9 Typical curves of the effect of discharge depth and temperature on battery life)



Source: Pinho e Galdino (2014)

3.3.7 Advantages and Disadvantages

The main advantage of lead-acid battery is its low cost compared to other rechargeable battery technologies. On the other hand, lead-acid technology has its biggest villain in weight. The

following are the main advantages and disadvantages of lead-acid batteries available in various literature:

Advantages:

- a) Low cost and ease of production.
- b) Available in a wide range of sizes and capacities (from 2Ah to 3000Ah).
- c) Good performance for high discharge rates ($>1000\text{A}$).
- d) Moderate performance at low ($<0^{\circ}\text{C}$) and high temperatures ($>45^{\circ}\text{C}$).
- e) Electrically efficient (coulombic efficiency higher than 95%).
- f) High voltage cell (open circuit voltage greater than 2V).
- g) Good performance when on a float.
- h) Available in maintenance-free versions (without water replacement).
- i) Components are easily recycled (approximately 95% of materials are recyclable).

Disadvantages:

- a) Relatively low cyclical life, however, up to 2000 cycles can be obtained with special projects.
- b) Limited specific energy of the order of 30 to 40 Wh.kg^{-1}
- c) Long-term storage (over 3 months) with the battery discharged can lead to irreversible phenomena such as sulphation, a phenomenon characterized by the formation of lead sulfate crystals in the active material of the plates of a lead-acid battery.
- d) Difficulty in manufacturing in very small sizes.
- e) The evolution of hydrogen in some projects results in explosion risk.

4 Charge Controllers

Charge controllers regulate the power coming from the photovoltaic modules to prevent the battery from reaching the overload state. Disconnecting the battery to prevent it from reaching a very low voltage is also a crucial function of the charge controller (KALOGIROU, 2013). Charge controllers are critical components in isolated photovoltaic systems, because if they fail, the battery may suffer irreversible damage (PINHO; GALDINO, 2014).

The charge controller is the link between the photovoltaic module, the battery and the charge. Some of its main requirements are: low internal consumption ($<5\text{mA}$), high efficiency (96 to 98%) and disconnection of charge in case of deep battery discharge (LUQUE; HEGEDUS, 2011). Among the main desirable features are: three stage charging and maximum power point tracking, MPPT (PINHO; GALDINO, 2014).

Modern controllers for isolated photovoltaic systems are microprocessor-based power electronics that operate in Pulse Width Modulation (PWM) and charge the batteries in the following stages: coarse, adsorption and fluctuation, which may include a fourth phase, equalization, as illustrated in [Figure 4.1](#).

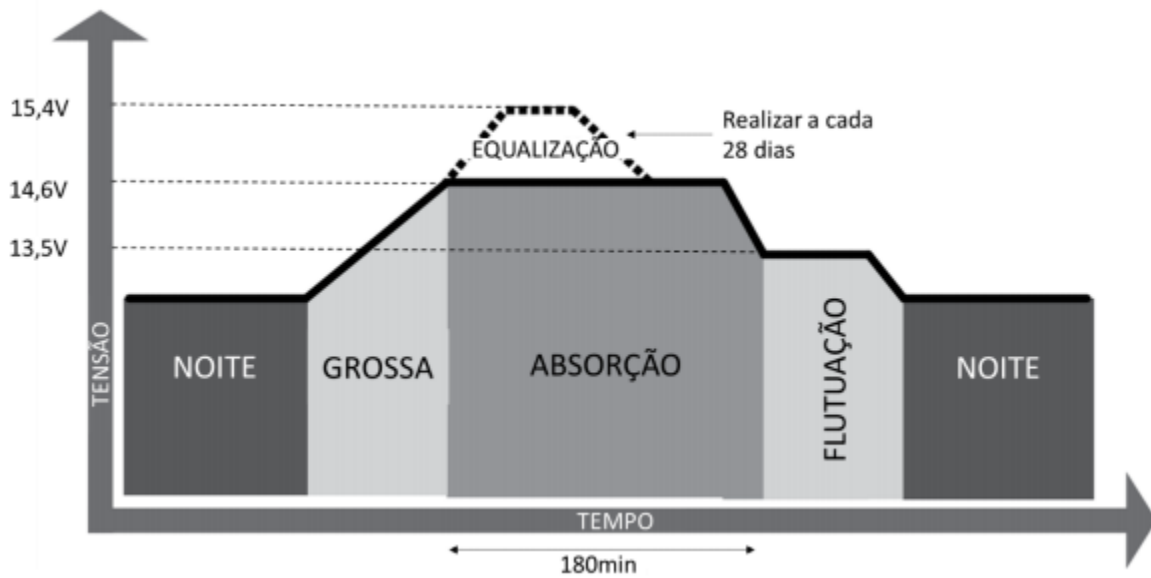
In the Coarse phase, which characterizes the start of charging, when the battery is discharged, the controller applies to the batteries the maximum current that the photovoltaic module can provide, until they reach a pre-established end of charge voltage. In the thick phase, 80-90% of the capacity is restored.

In the Absorption phase the battery voltage is kept constant at the end of charge voltage for a certain period of time until the battery is considered fully charged. The current supplied by the photovoltaic module is controlled in PWM and is gradually reduced.

In the Float phase the battery voltage is also kept constant with the current controlled in PWM, however, at a level that is much lower than the voltage of end of charge. This phase is maintained indefinitely until the battery discharges and its voltage stays below the fluctuation voltage for a certain period of time, when then a new cycle of coarse charge will be fired.

Equalization is a phase in which the controller applies a higher voltage to cause a controlled overload in the battery and obtain a bubbling in its electrolyte, a result of the gasification generated inside the battery. It is recommended by the manufacturers of both the battery and the charge controller that this charge occurs every 28 days to homogenize the electrolyte and prolong the life of the battery.

(Fig.4.1 Charge algorithm of a commercial charge controller. Thick phase, absorption, fluctuation and equalization)



Source: Morningstar, 2018.

4.1 Inverter

An inverter is an electronic device that supplies alternating current (AC) power from a direct current (DC) power source (PINHO; GALDINO, 2014). The inverters can be connected to the concessionaire's power grid or isolated.

Inverters for isolated photovoltaic systems must meet important requirements such as: input voltage between 12V and 48V, output voltage as close as possible to sinusoidal standard, low fluctuation in output voltage and frequency, high efficiency in case of partial load, withstand overload for equipment start-up conditions (e.g. refrigerator) and withstand short circuits (LUQUE; HEGEDUS, 2011).

Inverters of the type connected to the grid must additionally have their parameters synchronized with those of the power utility network (voltage, frequency, etc.) (PINHO; GALDINO, 2014).

5 State of Charge (SOC)

The State-Of-Charge (SOC) charge state of a battery is defined as the ratio between the difference in the nominal capacity and the amount of charge taken from the battery since its full charge state, at the nominal capacity, as follows

$$SOC = \left(\frac{C_{nominal} - C_{removed}}{C_{nominal}} \right) \times 100\%, \quad (5.1)$$

in which $C_{nominal}$ is the nominal capacity and $C_{removed}$ is the quantity of load withdrawn in the discharge.

Estimating the state of charge is one of the most important issues in battery applications. Accurate SOC estimation provides efficient battery utilization and stable battery management, preventing the system from an unexpected interruption as well as extending battery life. Many systems are sensitive to deep discharge or overcharging conditions because an excessively high or low SOC can cause irreversible damage to the battery. (PILLER, 2001)

The battery object of this work is lead-acid technology, a technology that has reached the stage of maturity and has been used in several engineering applications. Lead-acid batteries continue to be the main energy storage unit for applications in hybrid electric vehicles and photovoltaic systems. Ideally, lead-acid batteries commonly used in microgeneration systems should never be discharged below 50% of their nominal capacity. However, after a discharge close to 50% of their nominal capacity, the batteries should be fully recharged before the next discharge cycle. Usually, it is assumed that batteries are best operated in high SOC's to optimize their service life. To protect the battery from deep discharges, manufacturers recommend a limit of 80% SOC, which when reached should be fully recharged before the next discharge. Deep discharges reduce

the cyclic life of the battery by approximately 75% over the life of a battery that experiences a minimum state of charge of 80% during the cycles. (MOURA,2017)

5.1 SOC monitoring methods for lead acid batteries

Lead acid batteries are used in a number of applications requiring high reliability, robustness and predictability. A reliable state-of-the-art estimation strategy is necessary for uses such as hybrid vehicles, electric vehicles and telecommunications power supplies, and therefore several ways of estimating SOC are widely known in the industry. Accurate SOC estimation methods may prevent the battery from being deeply discharged or often overcharged, both of which significantly reduce the battery life remaining. Before the methods are presented, it is important to state the accuracy of the SOC estimation required for the different battery applications.

The battery serves as a starter for the motor in Hybrid Electric Vehicles (HEV) and any SOC readings which are not precise with an error of more than 5 percent will seriously affect the fuel output of the engine and the motor operations. For this reason, the SOC estimation in HEV applications must be as accurate as possible, with an error value never exceeding 5% of the measurement capacity.

However, the battery SOC determines the distance the vehicle can travel in (EV). The SOC battery in electric vehicles resembles the conventional vehicle fuel tank, which is notoriously imprecise (usually about 5 percent measurement error) so that the borderline of 5 percent -7 percent errors in EV applications may be appropriate. It is important not to misunderstand the battery capacity with SOC while designing the state of charge estimation method. SOC estimation depends on the battery aging process and after a certain number of charging / discharging cycles 20 percent or greater error will occur. For the following reason, the estimation of battery's state of charge should be battery's energy content and power capability.

The estimation of the SOC of the battery has more or less complexity depending on the type of battery and the application in which the battery is being used (PILLER; PERRIN; JOSSEN, 2001). The various mathematical methods for estimating SOC are classified according to the methodology. The estimation methods are divided into four categories (WATRIN; BLUNIER; MIRAUI, 2012; PRAJAPATI et al., 2011):

- (i) **Direct Measurement:** Physical properties such as voltage, and impedance of the battery is used in this method.
- (ii) **Book-keeping Estimation:** Discharging current as input and to calculate SOC integrates the discharging current over time.
- (iii) **Adaptive Systems:** Various new adaptive systems are used for the calculation of SOC now a days. These are the self-designing and can automatically adjust the SOC for different discharging conditions.
- (iv) **Hybrid Methods:** The hybrid methods produce good estimation of SOC as compared to other methods used individually. These methods allow a globally optimal estimation performance.

(Table 5 presents the specific mathematical methods for estimating SOC by category)

Categories	Mathematical Methods
Direct Measurement Method	Open circuit voltage method
	Terminal voltage method
	Impedance method
	Impedance spectroscopy method
Book-keeping Estimation	Coulomb counting method
	Modified Coulomb counting method
Adaptive Systems	BP neural network
	RBF neural network
	Support vector machine
	Fuzzy neural network
	Kalman filter
Hybrid Methods	Coulomb counting and EMF combination
	Coulomb counting and KF combination
	Per-unit system and EKF combination

Source: Chang (2013)

5.2 Kalman Filter

In 1960, Rudolf Kalman published an article in which he proposed a solution recursive to the problem of discrete linear signal filtering that remained widely known as the Kalman filter (BISHOP et al., 2001). The Kalman consists of a set of mathematical equations which provide an efficient computational means to estimate the state of a process in a way recursive. The purpose of the filter is to extract information from data that contain noise, uncertainty or error (RHUDY; SALGUERO; HOLAPPA, 2017).

The Kalman filter was designed to operate in systems represented in the discrete linear state space format, i.e. systems of the form

$$x_k = Ax_{k-1} + Bu_{k-1} + w_{k-1}; \quad (5.2)$$

$$y_k = H_k x_k + v_k; \quad (5.3)$$

where A is the system matrix, B is the input matrix, u is the vector representing the system input, x is the system state vector, H is the state measurement matrix, and y represents the system output vector. The variables w_{k-1} and v_k are random and represent the process and measurement noise, respectively. They are assumed to be independent variables. The dynamics of the system states are described by (5.2) while (5.3) describes the system output (BISHOP et al., 2001).

The state vector, x , is composed of the state values estimated by the filter. An important distinction between vector x and vector y (output) is that, commonly, the system output is the result of interest, however, for state estimation problems using Kalman filters, the states, i.e., vector x , are the desired results. The output vector, y , is composed of measurements physically made in the system that are transformed for later comparison with the estimated filter states. This comparison

is the parameter that the filter uses to correct its state estimation (RHUDY; SALGUERO; HOLAPPA, 2017).

The input vector, u , contains the input information that defines system dynamics. Its value can be derived from sensor measurements. Matrices A , B and H vary according to the problem and are used in the equations of a linear system depending on their states and inputs. Generally, these matrices are composed of constant values (RHUDY; SALGUERO; HOLAPPA, 2017).

5.3 Algorithm of Kalman Filter

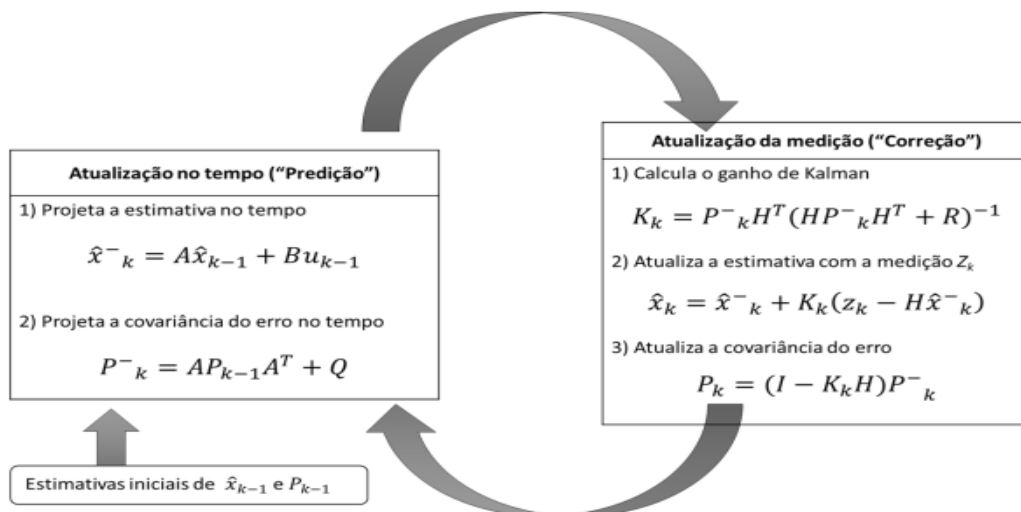
The Kalman filter performs a prediction followed by a correction based on measurements (with noise) to estimate the system states, i.e. the filter estimates the process using a form of feedback control (BISHOP et al., 2001).

The Kalman filter equations are divided into two groups: time update equations and measurement update equations. The update time equations are responsible for projecting the estimates of the current state and covariance over time to obtain the so-called a priori estimate. The update equations of the measurement are responsible for feedback, i.e., for incorporating a new measurement into the a priori estimate to obtain an improved a posteriori estimate. The update equations in time are also defined as prediction equations, while the update equations of the measurement are defined as correction equations (BISHOP et al., 2001). The equations that make up the filter algorithm, illustrated in Figure 5.1, are presented below.

In general, the Kalman filter estimates the state $x \in \mathfrak{R}n$ of a discrete process that is governed by (5.2), with measurement $z \in \mathfrak{R}m$, given by

$$z_k = Hx_k + v_k. \quad (5.4)$$

(Fig. 5.1 Kalman filter recursive algorithm)



Source: Bishop et al., 2001

In the algorithm equations illustrated in Figure 5.3, the minus sign in the variable indicates that it is an a priori estimate, that is, before the correction. The circumflex accent above the variable indicates that it is a vector. As an example, the variable \hat{x}^-_k represents the vector of estimated states at instant k.

In the algorithm in Figure 5.3, the first step is to estimate the state vector by

$$\hat{x}^-_k = A\hat{x}_{k-1} + Bu_{k-1}; \quad (5.5)$$

from initial estimates for the vector \hat{x}^-_k .

Then the covariance matrix of the estimate error, P, is estimated by

$$P^-_k = AP_{k-1}A^T + Q; \quad (5.6)$$

from initial estimates of P, in which Q is the covariance matrix of process noise.

Once the estimates have been defined, the Kalman (K) filter gain matrix is calculated by

$$K_k = P^-_k H^T (HP^-_k H^T + R)^{-1}; \quad (5.7)$$

where R is the covariance matrix of the measurement noise, P is the covariance matrix of the estimate error and H is the state measurement matrix of the system.

The state vector is then corrected by weighting the term $(z_k - H\hat{x}^-_k)$ by the filter gain matrix, as per

$$\hat{x}_k = \hat{x}^-_k + K_k(z_k - H\hat{x}^-_k); \quad (5.8)$$

The term $(z_k - H\hat{x}^-_k)$ is defined as the measured or residual innovation, where z_k is the obtained measurement and $H\hat{x}^-_k$, the estimated measurement, being \hat{x}^-_k determined by (5.5).

Similarly, the covariance matrix of the estimate error, P, is corrected according to

$$P_k = (I - K_k H)P^-_k. \quad (5.9)$$

After executing an algorithm cycle, an estimate of the system states is obtained, represented by the vector \hat{x}_k , which is the result of interest; and the covariance matrix of the estimate error, represented by P_k . The algorithm is then run again, taking as input the estimated values.

5.4 State of the Art

As presented earlier in this chapter, Kalman filter is an algorithm for estimating the internal states of a dynamic system. In our case, the battery is the dynamic system and the internal state is the SOC (PILLER; PERRIN; JOSSEN, 2001). Gregory L. Plett was the pioneer in the use of Kalman filter for battery equivalent circuits (RAHN; WANG, 2013).

Bhangu et al. (2005) used the Kalman filter technique to estimate the SOC of a 2V lead-acid battery and 6Ah capacity in 8 hours, of AGM technology, subjecting it to standard loading and unloading cycles taken from Hybrid Electric Vehicles (HEV) use profiles. The results showed an approximate 2% error for SOC when estimated by Kalman filter; in contrast, for the coulomb-counting technique, the error shown was of the order of approximately 15% for the same cycles loading and unloading patterns.

Generally, the kalman filter is limited to linear processes, thus being, Vasebi et al. (2007) and Benila, Vasantharathna and Geetha (2014) used the Extended Kalman Filter based technique (EKF), which consists of the linearization of a nonlinear state space model, as is the case with the battery. Vasebi et al. (2007) submitted the lead-acid battery of 2V and 6Ah capacity to standardized load and unload cycles and the estimation of the SOC by the dynamic method (EKF) showed a difference of 3% when compared to the static method of measuring internal resistance to estimate the SOC, the method used by the vehicle system used in the study. Benila, Vasantharathna and Geetha (2014) report errors of the order of 2% in the simulation of the SOC estimation of lead-acid batteries using the EKF technique.

Piao et al. (2010) used the Kalman unscented filter technique (UKF) which also uses a nonlinear transformation algorithm. The lead-acid battery was subjected to three usage profiles, namely constant current, constant voltage (large scale current variations) and loading and unloading pulses. For the profile of constant current, the average error of the SOC estimate was less than 1%. The profile of constant tension showed an average error of 5% up and down. Finally, the loading and unloading pulse profile showed a maximum error of 10%.

Marchildon, Doumbia and Agbossou (2015) implemented a method called the Two-Pulse Charge Test in a laboratory and validated it on a 180Ah (C20) lead-acid ventilated battery. The method requires about 5 minutes for SOC estimation.

Loukil, Masmoudi and Derbel (2017) implemented the SOC estimator in an Arduino microcontroller and conducted experimental laboratory tests with a 7Ah capacity VRLA 12V battery. The work of Loukil, Masmoudi and Derbel (2017) is quite similar to this work, however, the battery used is of low capacity VRLA technology and the tests were conducted in laboratory and not in the field.

Costa, Araujo e Carvalho (2016), Ting et al. (2014) and Benila, Vasantharathna and Geetha (2014) estimated the SOC through the technique of filters of Kalman for batteries of different technologies in simulation environment. Bhangu et al. (2005), Vasebi et al. (2007) and Loukil, Masmoudi and Derbel (2017) obtained satisfactory experimental results in the laboratory using the same technique applied to lead-acid batteries of the VRLA type for automotive applications, in the cases of Bhangu et al. (2005) and Vasebi et al. (2007), specifically.

6 MATERIALS AND METHODS

This chapter presents the materials used in the study as well as the methods applied to estimate the state of charge of the lead-acid battery.

6.1 Material

6.1.1 Studied Photovoltaic System

The isolated photovoltaic solar system studied was a solar pole located in the parking lot of the Distribution Center of the company Acumuladores Moura S/A, located in the city of Belo Jardim, interior of the state of Pernambuco, whose average annual temperature is 30°C.

Besides batteries, the system consisted of photovoltaic modules, luminaries and charge controllers whose main technical information is presented in Annex A. [Figure 6.1](#) presents an image of the photovoltaic pole used in the study.

According to the project, which was not part of the scope of this work, each pole consists of two independent solar systems. Each solar system consists of 01 panel, 01 charge controller, 01 battery and 01 luminaire. To this job, only one of the solar pole systems had its battery instrumented for the state of charge estimation study. The battery was lead-acid, stationary and ventilated type. [Figure 6.2](#) shows the diagram of blocks of the solar pole studied.

(Fig.6.1 Solar pole used for battery study)

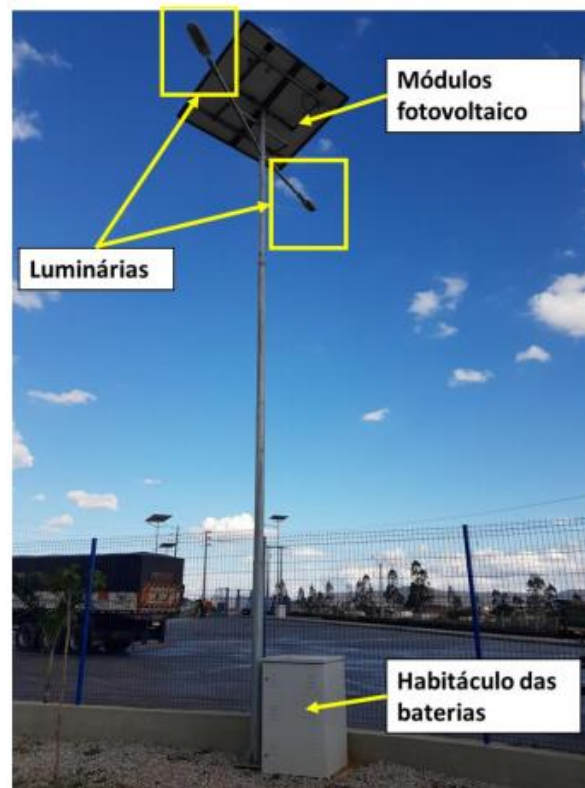
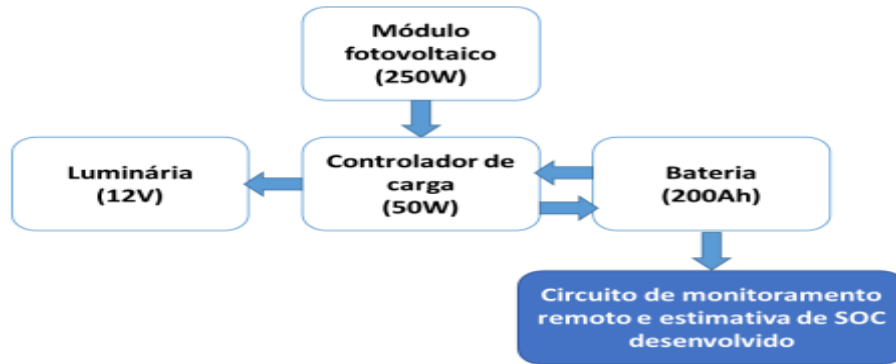


(Fig.6.2 Solar pole block diagram studied)



6.1.2 Electronic Circuit

The electronic remote monitoring circuit responsible for estimating the state of charge of the battery was developed on the Arduino platform with the model MEGA2560. One premise for this circuit, since it was powered by the battery of the isolated photovoltaic system itself, was that its energy consumption should be minimal so as not to represent a considerable load for the system. The impact of the circuit consumption on the system was evaluated in relation to the state of charge experienced by the battery at the end of daily discharges with and without the circuit installed in the system.

The circuit was installed on the solar pole and, as will be seen below, through specific sensors measured system quantities such as voltage, current and ambient temperature. In addition to the sensors, the circuit was equipped with some peripheral devices as illustrated in the block diagram in [Figure 6.3](#).

(Fig.6.3. Electronic circuit block diagram)

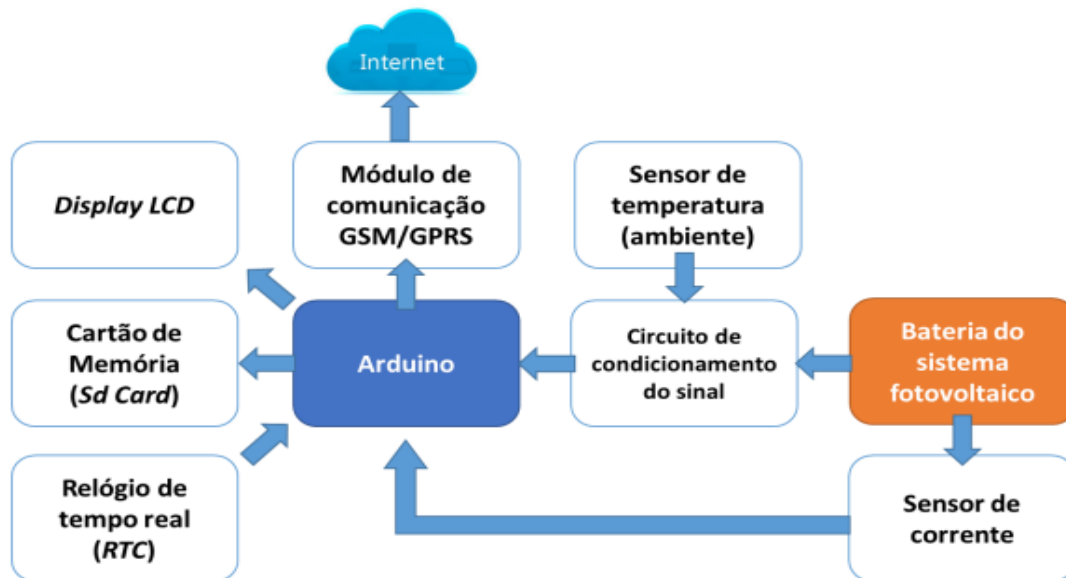


Figure 6.4 shows the electrical schematic of the signal conditioning circuit in addition to the peripherals of the microcontroller, such as the liquid crystal display of the Liquid Crystal Display (LCD), the Secure Digital Card SDcard, and the Real Time Clock (RTC). The circuitry in **Figure 6.4** is repeated in Appendix E in a larger manner for better viewing.

The sensors used are to measure the constant electrical current (C.C.) and temperature quantities. The current sensor is the integrated circuit ACS712 that uses the hall effect and allows to measure electrical current in both directions, having its maximum nominal values of $\pm 20\text{A}$. The temperature is monitored through the LM35 sensor, a precision integrated circuit whose output voltage is linearly proportional to the temperature in degrees ($^{\circ}\text{C}$). For the signal conditioning circuit the LM324 integrated circuit from the manufacturer Texas Instruments was used, which is composed of four operational amplifiers that have the characteristic of no generate polarizing voltage at their outputs when their inputs are zero (TEXAS, 2015), allowing the entire 10-bit resolution of Arduino's analog-to-digital converter to be used for the range of interest values of the magnitude sampled in question. To ensure the maximum possible resolution, the following were configured gains in the operational amplifiers suitable for each greatness.

Figure 6.5 presents the structured circuit for monitoring voltage, current and battery SOC estimate as well as ambient temperature monitoring, with data storage on memory card.

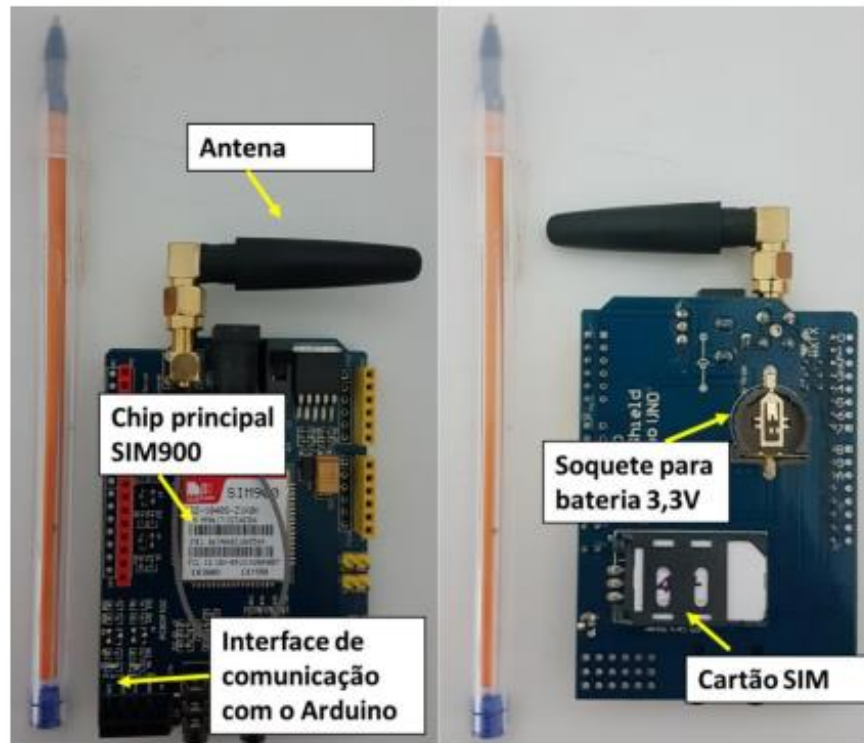
The communication system for remote monitoring was implemented with the aid of the GSM/GPRS SIM900 module. The module allows the exchange of data using the GSM cellular network of the English Global System for Mobile communication, i.e. through specific commands it is possible to send text messages to any mobile phone number as well as providing data to the Internet through the GPRS service of General Packet Radio Service. For the module to work properly it is necessary to equip it with a card valid SIM, from Subscriber Identify Module, with a mobile phone account active. At your installation site, telephone service must be available mobile. **Figure 6.6** presents in detail the GSM/GPRS SIM900 module.

Figure 6.7 and **Figure 6.8** present, respectively, the complete circuit for remote monitoring of the batteries and the internal view of the battery compartment on the solar pole, detailing its components and connections.

The MATLAB mathematical software was used for data treatment and battery parameter calculations, as well as simulations to validate the Kalman filter method to estimate the state of charge.

(Fig.6.4 Electrical schematic of the structured circuit for battery monitoring)

(Fig.6.6 SIM900 GSM/GPRS communication module)



(Fig. 6.7 Electronic circuit implemented for remote monitoring of battery charge status)

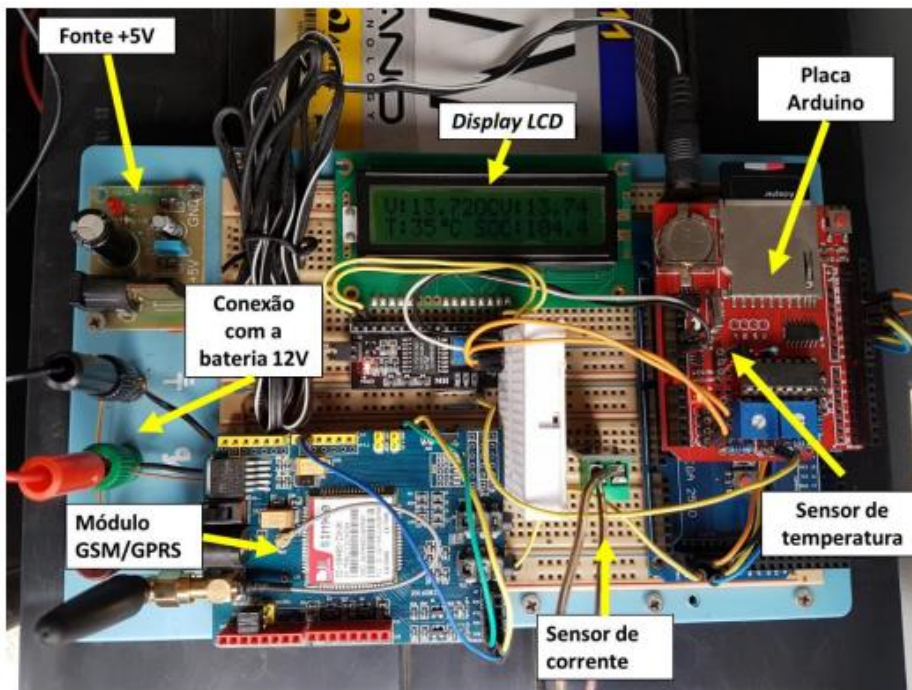
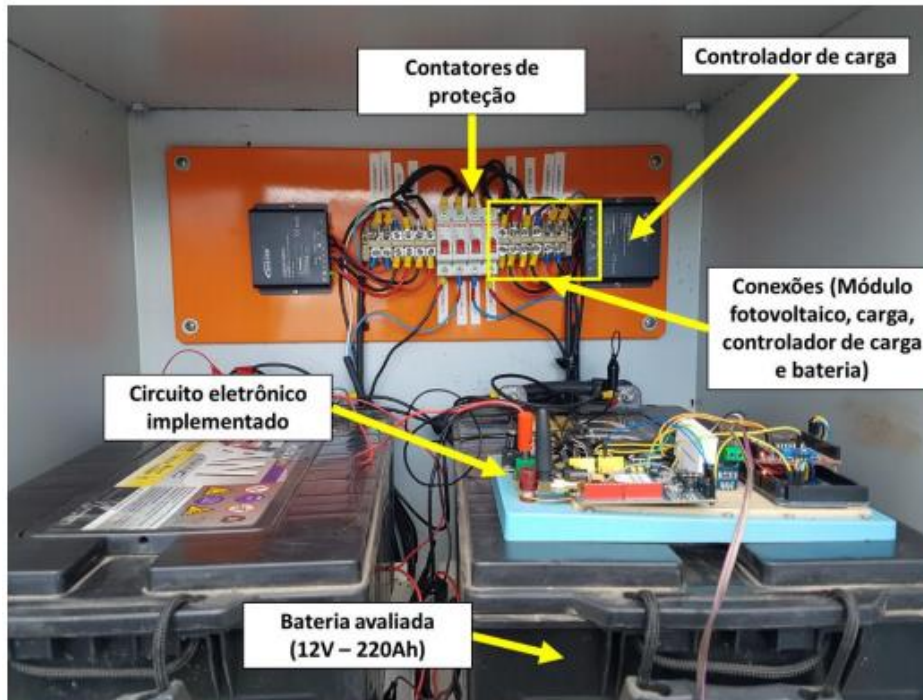


(Fig.6.8 Internal view of the battery compartment (components and connections))



6.2 Methods

The method chosen for estimating the state of charge (SOC) of the lead-acid ventilated stationary battery was the Kalman filter method due to its low memory and computational capacity requirements (PEI et al., 2017), since the algorithm is embedded in a low-cost microcontroller; besides being quite appropriate for batteries of photovoltaic systems and calculating in real time the state of charge of the battery (CHANG, 2013).

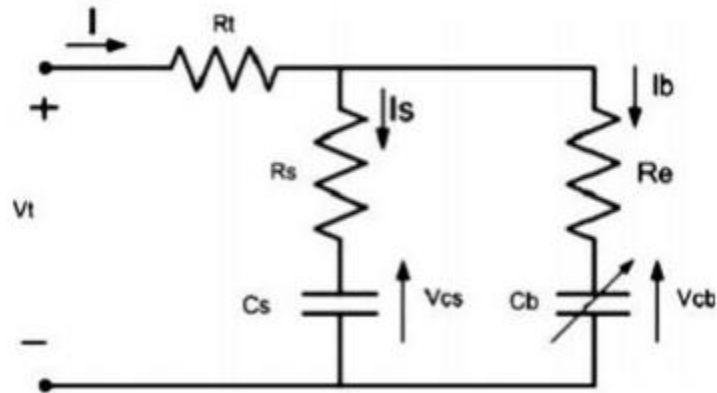
As seen in Section 3.2, the Kalman filter was designed to operate in systems represented in the discrete linear state space format, thus, to estimate the SOC per Kalman filter a dynamic model of the battery is required, in the form of state variable equations (BHANGU et al., 2005). The Kalman filter estimates internal states of the battery model that can be gauged only through complex techniques such as impedance spectroscopy (CHANG, 2013). These internal states, as presented in Item 4.2.1, have correlation with the state of charge of the battery.

6.2.1 Battery Model

Figure 6.9 shows the generic CR model of the battery proposed by Johnson, Pesaran and Sack (2000). In the RC model of the battery the capacitor C_b (C_{bulk}) characterizes the battery's ability to store charge, while C_s ($C_{s\ Surface}$), models the surface capacitance and diffusion effects within the cell. The voltage of the capacitances C_b and C_s is V_{cb} and V_{cs} , respectively. V_t or V_0 is the voltage

in battery terminals or output voltage. In this model, the charging current is positive, and the discharge current is negative.

(Fig.6.9 Battery RC model)



Source: Vasebi et al., 2007

The calculation of the parameters is initially carried out from data experiments from actual battery capacity tests in regime nominal (C10) and the relationship between the SOC and the open circuit voltage (OCV).

(Fig.6.10 Batteries under test in the thermostatic bath)

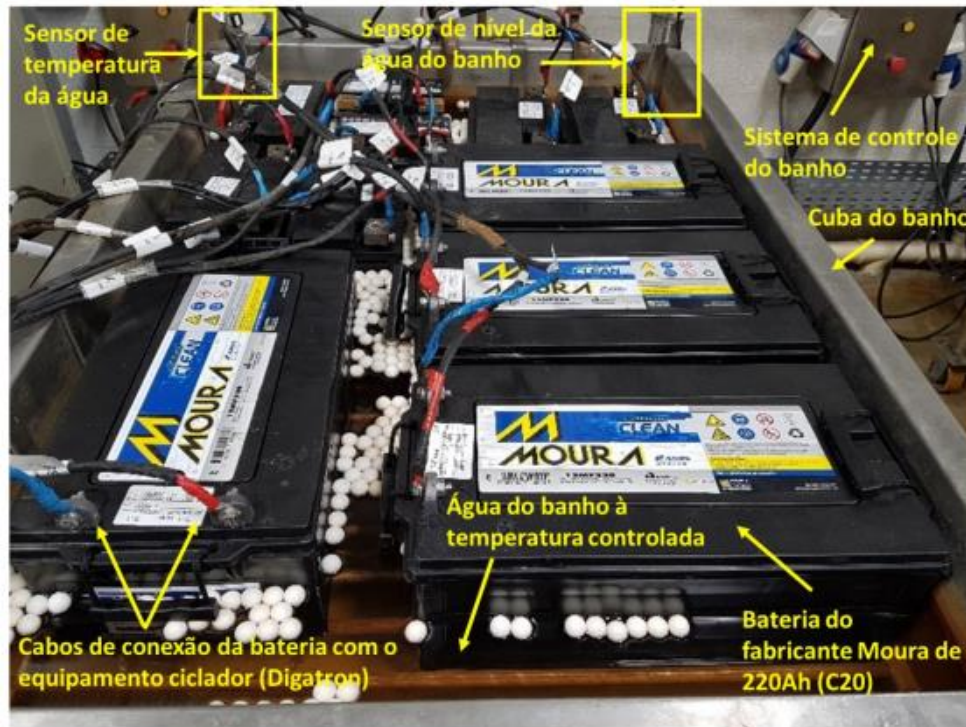


(Fig. 6.11 Simplified connection diagram between battery cycling equipment, computer and test batteries)



7. Results

This chapter presents the experimental results of the method for battery modeling as well as the results of simulations and field tests performed using the Kalman filter to estimate the state of charge of vented lead-acid stationary batteries.

7.1 Battery Design

7.1.1 Pre-treatment Test

For the pre-treatment test, the battery capacity of 200Ah in 10-hour regime was subjected to 04 discharges with constant current, equal to 20A (200Ah/10) until the battery reaches 10.5V. **Figure 7.1** shows the graph complete loading and unloading of the previous treatment. It is noted that during the two-hour break after 24 hours of recharging, the battery voltage tends to stabilize at the open circuit voltage value for the 100% state of charge, around 13V. After each recharge, the open circuit voltage increases. This behavior justifies the need for prior treatment aimed at stabilizing the battery capacity. Figure 7.3 shows the battery voltage curves overlapping for each of the discharges made into the sample. The results of the C10 capacities obtained are presented in Table 7. In Table 7 it is an increase in battery capacity can be observed with each discharge. This is if justifies the fact that the active battery material has not been completely transformed in PbO₂, for the positive plate, or Pb, for the negative plate, during the training in its manufacture, with this transformation taking place during the consecutive pre-treatment reloads (PINHO; GALDINO, 2014), already that it was a newly manufactured battery.

(Table. 7. Results of capacity tests (C10) during pre-treatment of sample)

Sequência do ensaio	C10 (Ah)	Tempo de descarga até 10,5V	%C10 nominal (%)
1° C10	189,98	9h30m	95
2° C10	195,24	9h46m	98
3° C10	198,23	9h54m	99
4° C10	197,55	9h53m	99

7.1.2 Obtained Capacity Test

After the previous treatment, for the determination of the obtained capacity, it was discharge with current of C10, 20A, until the battery reaches the voltage of 10,5V. The capacity obtained is shown in Table 7.1.2 while **Figure 7.2** shows the battery voltage curve together with the state of charge curve (SOC) during the discharge which was obtained through the Coulomb-counting technique or integration of current in time, from the discharge current data collected by the automatic loading and unloading equipment, Digatron.

(Table.7.1 Capacity test result (C10) after pre-treatment)

Ensaio	C10 obtido	Tempo de descarga até 10,5V	%C10 nominal
Capacidade obtida	198,12Ah	9h55m	99%

(Fig. 7.1 Pre-treatment. Consecutive discharges for battery stabilization)

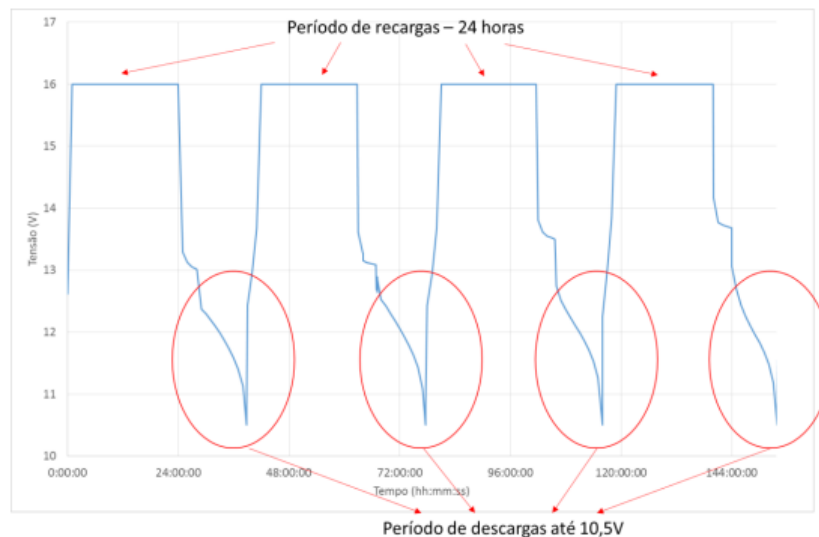


(Fig.7.2 Overlapping discharge curves of the pre-treatment sample)

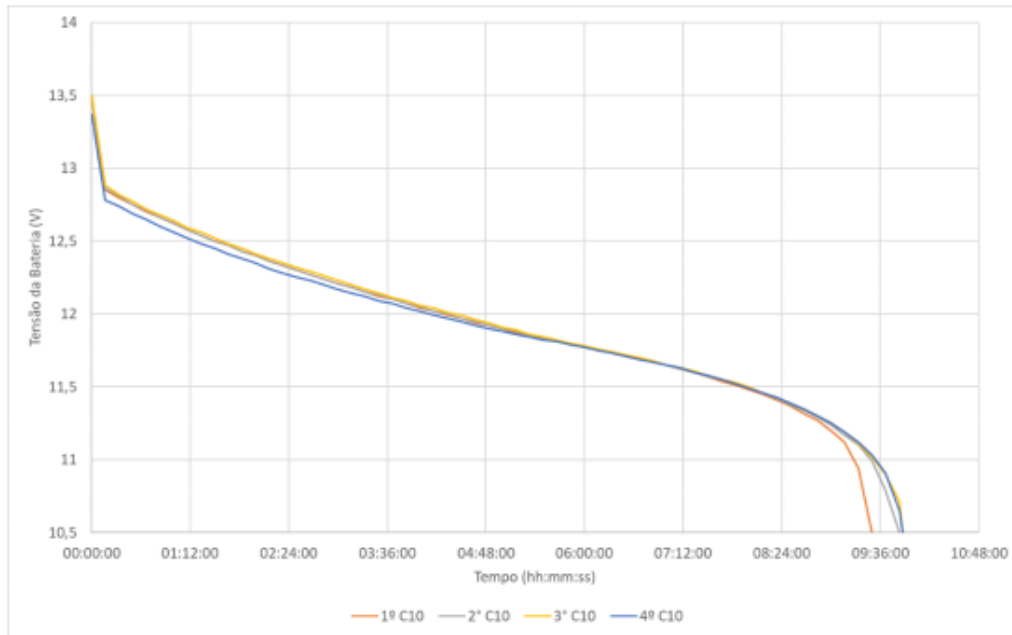
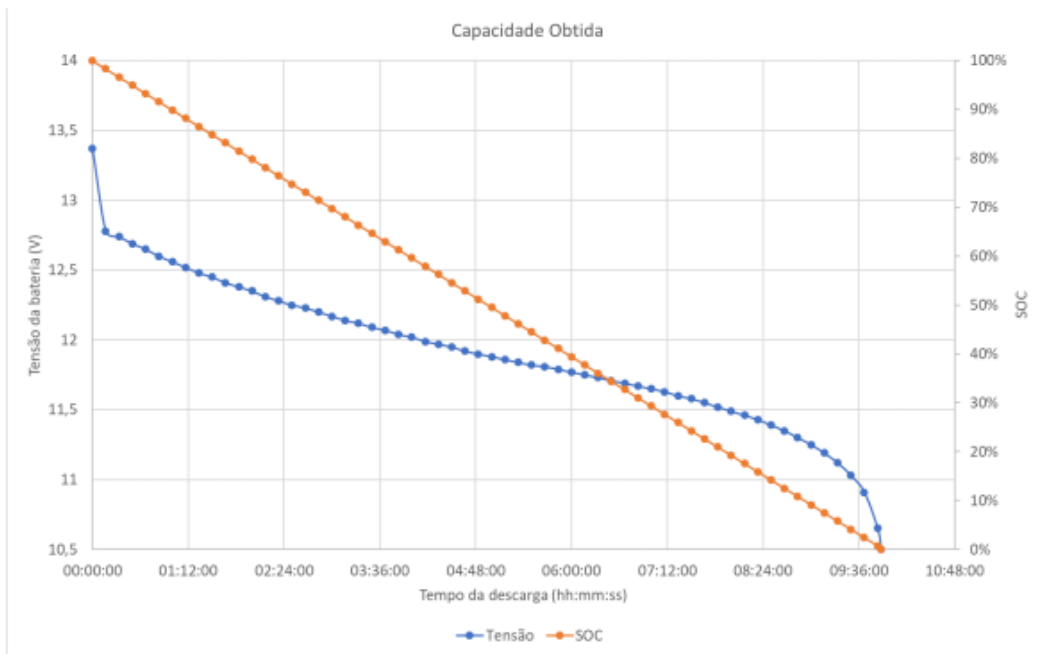


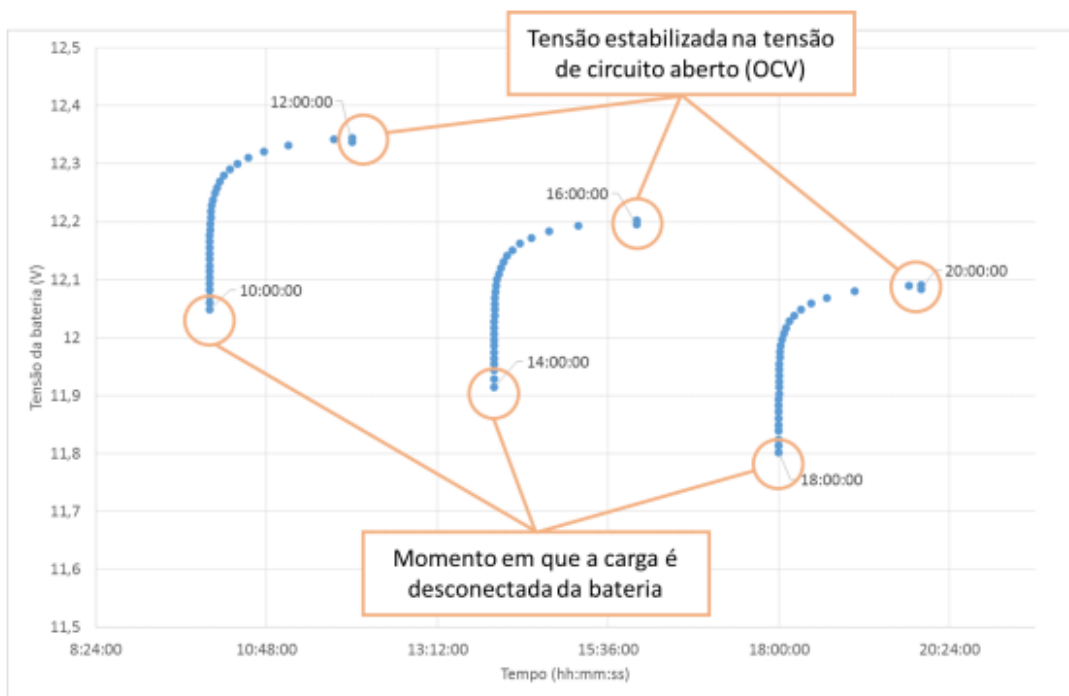
(Fig.7.3 C10 discharge curve overlapping battery state of charge (SOC) curve)



7.1.3 Test of Determination of VOC x SOC ratio

For the determination of the relation OCV x SOC a previous study was carried out to determine the average time needed for the battery to reach and stabilize the open circuit voltage at equilibrium value, OCV. **Figure 7.4** shows the curve of battery response from the moment the charge is disconnected, i.e. when the current is equal to 0A, until stabilization at the open circuit voltage value. An open circuit rest was performed in different states of charge, 70%, 60% and 50% of nominal capacity. It was observed that the battery took around of two hours until it stabilized its tension, as could be seen by the times in highlighted in the chart. This two-hour time was used for the rest of the battery between discharges interspersed in the curve determination procedure OCV x SOC, as shown below.

(Fig. 7.4 Response time until battery reaches open circuit voltage (OCV))



According to the method presented in Item 4.2.2.3, the battery was submitted to partial discharges of 1h with current of C10, interspersed with periods of 2-hour rest in open circuit, previously determined, for voltage stabilization in continuous state. Table 7.1.3.1 shows the values of OCV and SOC. **Figure 7.5** shows the voltage and SOC curves of the battery as a function of time. The SOC was calculated using the Coulomb-counting technique or integration of current in time. In Figure 5.5 it is possible to observe the degree of linearity the relationship between the CMO and the SOC, as observed in the literature. The behavior change observed in the 10% SOC region is justified by the lack of acid in the solution to react with the active material of the plates since, during discharge, as seen in Figure 2.7, the acid migrates to the plates and the solution, at

the end of the discharge, consists practically of water (LINDEN, 2011). The discharge was not performed until the 0%SOC state to avoid discharge the battery deeply.

(Fig.7.5 Partial discharges to determine the OCVxSOC relationship)

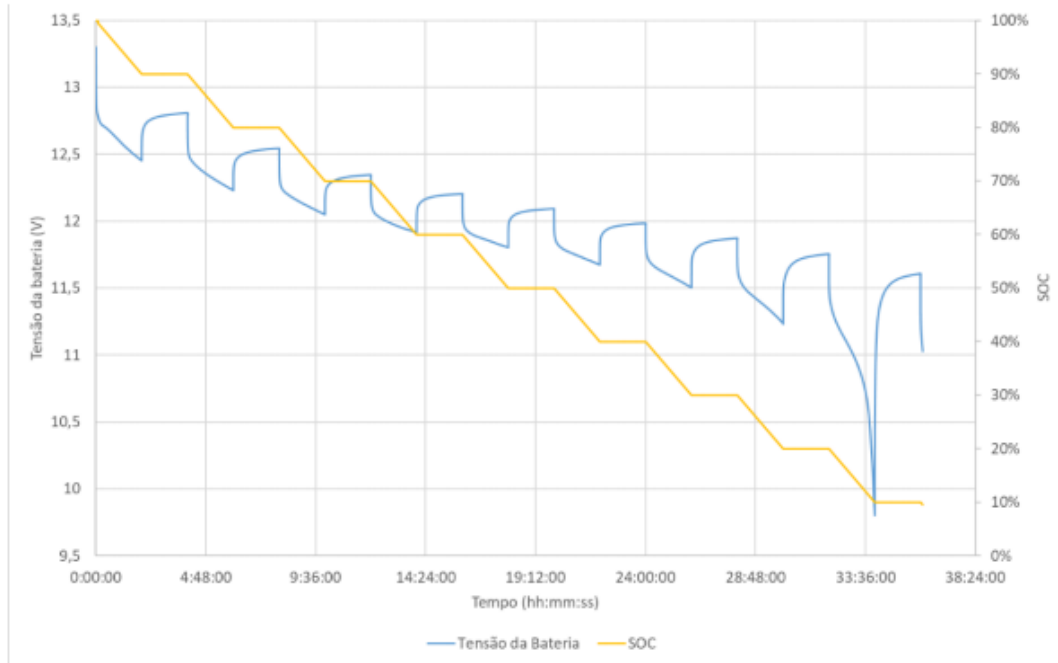
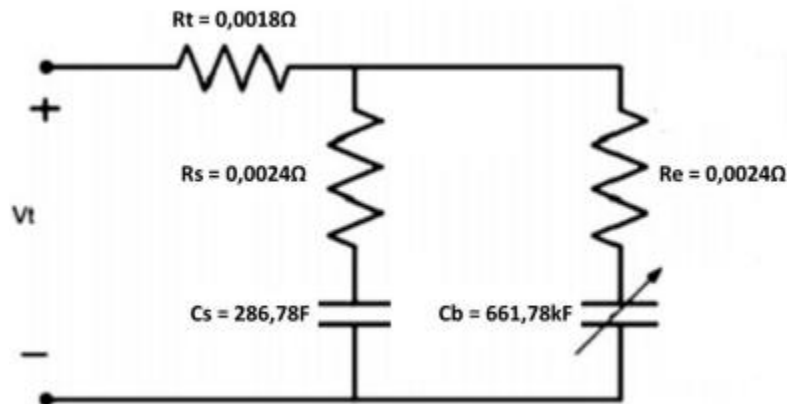


(Table. 7.2 OCV x SOC Relation)

OCV (V)	SOC (%)
13,10	100
12,80	90
12,53	80
12,33	70
12,20	60
12,08	50
11,97	40
11,86	30
11,74	20
11,58	10

7.1.4 Determination of battery model parameters

(Fig. RC Battery Model)



The C_{bulk} (C_b) capacitance, where the capacity used was the capacity obtained, according to [Table 7.3](#), converted from Ah to unit A.s (amper-second). The capacitance value of C_{surface} (C_s) was determined through the battery response to high-frequency excitement. The current of 22A (C20 current) in pulses of 500ms duration (Δt). The voltage response of the battery to the excitation profile can be seen in [Figure 7.6](#). According to presented in the method, by observing the voltage response curve of the battery, the voltages defined as V1, V2, V3 and V4 are determined, whose values found are shown in [Table 7.1.4.2](#) and shown in [Figure 7.6](#).

(Table. 7.3 Voltages taken from the battery's response curve to the high-frequency excitement)

Descrição	Tensão (V)
V1	12,94
V2	12,80
V3	12,90
V4	12,94

Battery resistance (R_m) was measured with internal battery resistance measuring equipment from the manufacturer Fluke, model BT521. The internal resistance measurement with this equipment is performed directly, that is, its terminals, positive and negative, are connected in the positive and negative poles of the battery, respecting the polarity, and in a few seconds the value of the internal resistance, in $m\Omega$, is presented in the screen of the equipment. To check the internal resistance of the battery, the equipment injects an alternating sine current signal with amplitude of 100mV and frequency of 1kHz (FLUKE, 2014). The measured resistance value of the battery (R_m) was 0.003 Ω .

(Fig.7.6 Battery voltage when excited by a 500ms long current pulse)

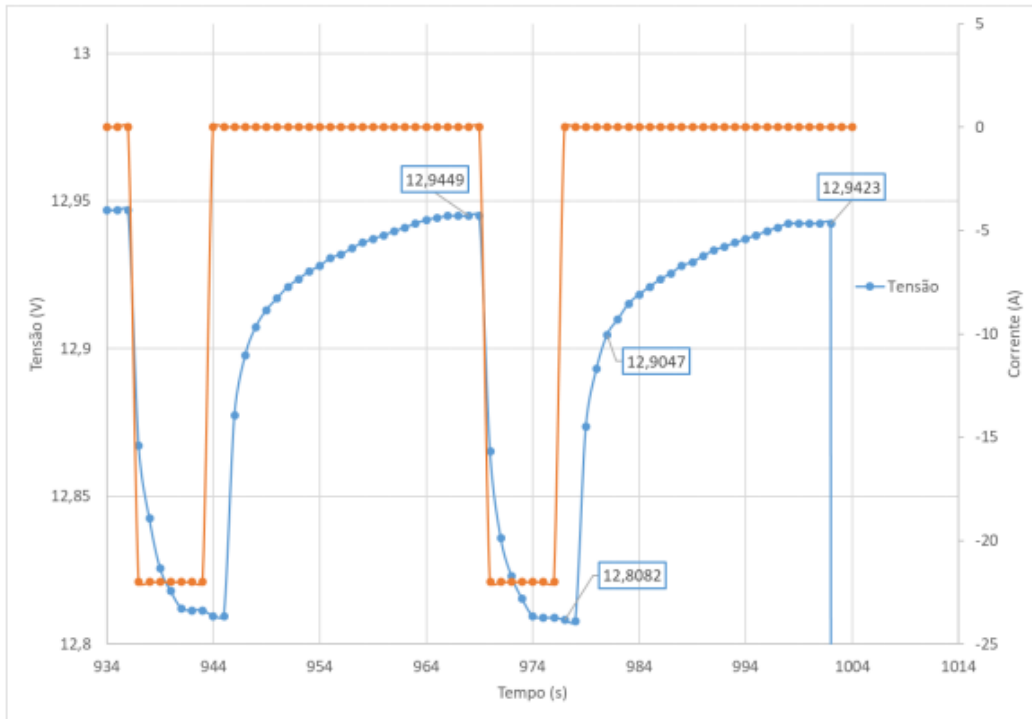


Table 7.4 shows the values found for all RC battery model parameters, namely C_b , C_s , R_e , R_s and R_t .

(Table.7.4 Battery RC model parameter values)

Parâmetro	$C_{bulk} (C_b)$ (F)	$C_{superfície} (C_s)$ (F)	R_e (Ω)	R_s (Ω)	R_t (Ω)
Valor	$661,78 \times 10^3$	286,78	0,0024	0,0024	0,0018

7.2 Estimation of SOC of the Battery

To check the Kalman filter algorithm using the calculated battery parameters, the simulation was performed in MATLAB software. Then, checking the validity of the parameters and the functionality of the algorithm, the tests were performed in the field, with the Kalman filter algorithm embedded in the developed remote monitoring circuit Arduino.

7.2.1 Simulation for SOC estimation

For the simulations, the Kalman filter algorithm was implemented in MATLAB whose lines of code are presented in Annex C. The simulations were performed with the discharge data from a C20 test and the OCV x SOC verification test. The results are presented from Figure 7.7 to Figure 7.12.

First, to validate the Kalman filter method as well as the battery model parameter values previously determined, the filter algorithm was subjected to input values equivalent to the voltages measured in the battery during the test performed to determine the OCV x SOC ratio. In **Figure 7.7**, it was observed that the filter followed quite faithfully the open circuit voltage values observed at the end of the battery rest period when the load was removed ($I = 0A$). In order to achieve this satisfactory result, it was necessary to test several random values for the covariances of process noise, Q , and measurement noise, R . The optimal values found are shown in Table 7.5. A high R -value means that the filter "relies" little on the measurement, which effectively means that the filter should correct less with each measurement update. The low Q value means that the system state equations have good accuracy (RHUDY; SALGUERO; HOLAPPA, 2017).

(Table.7.5 Optimum values of Kalman Q filter parameters and R)

Parâmetro	Valores
R	12×10^3
Q	$\begin{bmatrix} 10^{-8} & 0 & 0 \\ 0 & 10^{-8} & 0 \\ 0 & 0 & 10^{-8} \end{bmatrix}$

To validate the SOC results estimated in the simulation, a comparison was made with the SOC estimated by the current integration technique or Coulomb counting, which is a very reliable method when the initial load state condition is correctly established (PILLER; PERRIN; JOSSEN, 2001). Since the data used in the simulation came from a discharge test carried out on a fully charged battery, the initial charge state was considered 100%. In **Figure 7.9** it was possible to observe the SOC fidelity estimated by the Kalman filter against the SOC estimated by current integration. A behavior changes in the region close to 10%SOC is observed due to acid deficiency in the battery solution when its state of charge approaches 0% (PINHO; GALDINO, 2014).

Observed the satisfactory result of the SOC estimate in the profile of interleaving discharges, the filter was tested using discharge data of a capacity test in 20 hours, or C20. **Figure 7.10** shows the curves the battery voltage measured during the discharge of C20 and the open circuit voltage (OCV) estimated. The satisfactory response of the filter to the discharge of C20 is observed in **Figure 7.11**, where after stabilization of the filter, between the 95%SOC region and 50%SOC, the average absolute error has a maximum value around 2%. Errors above 5% are observed in the region of state of charge below 40%SOC. Figure 5.13 presents an enlarged view of the graph in **Figure 7.11** in the stabilization region from the filter. It can be seen that the filter takes around 1672 seconds, or 28 minutes, to have SOC errors estimated below 5% when compared to the SOC estimated by current integration.

Despite the average absolute error of 2% observed in the simulation of the estimation of the SOC in the region of the curve between 93%SOC and 50%SOC, it was realized that the Kalman filter was able to estimate the SOC in a way to provide an analysis reliable usage profile to which the battery is being submitted, i.e., although of the average error, it is possible to identify whether the battery is experiencing scenarios that contribute to the reduction of their useful life, such as

cycling in low state of charge (SOC < 50% of nominal capacity) and rarely experience full load (ZHAO, 2013). This strengthens the applicability of the Kalman filter for estimating SOC of photovoltaic system batteries in view of the fact that, in this type of system, the Battery discharge depth should not exceed 50% (ZHAO, 2013), causing the filter to work in the lowest error region.

(Fig.7.7 Estimated OCV compared to the voltage measured in the test to determine the relationship between OCV and SOC)

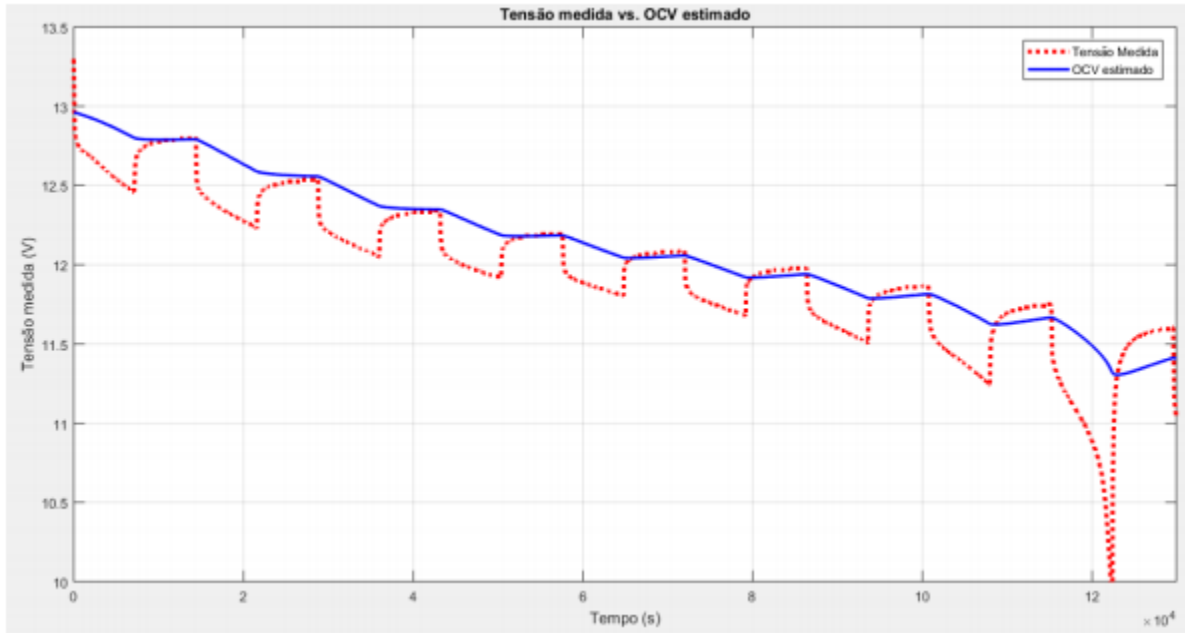


(Fig.7.8 Extended view of Kalman filter behavior when estimating OCV)

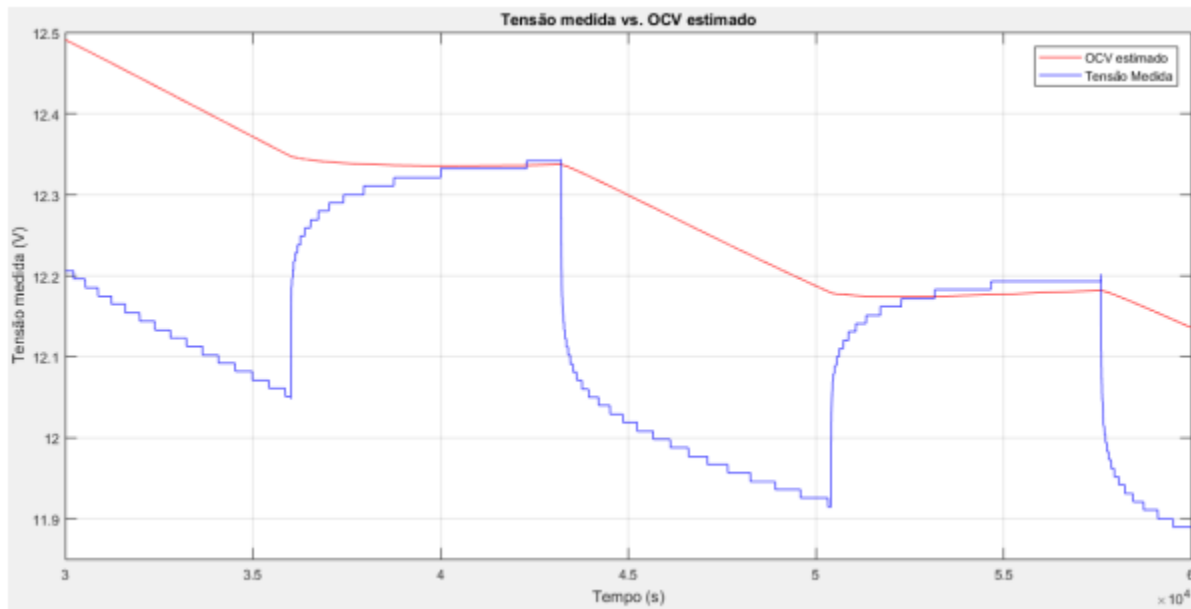


(Fig.7.9 Comparison between estimated SOC and SOC by current integration for the curve of the OCV x SOC ratio test)

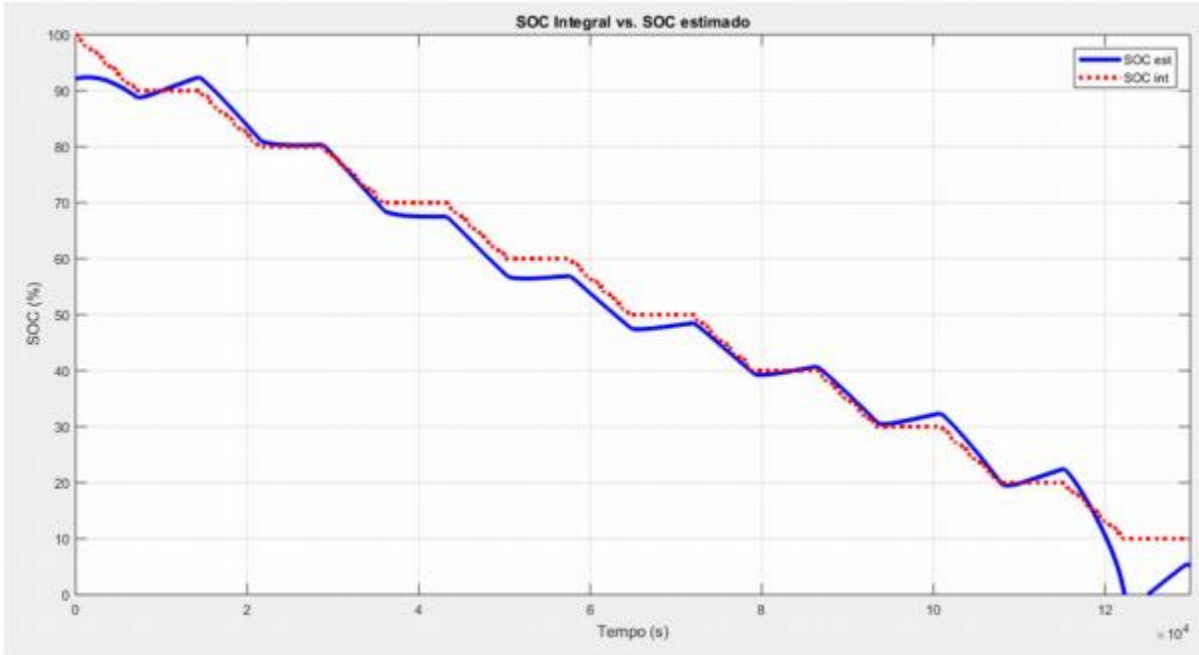


(Fig.7.10 Battery voltage curve measured during C20 discharge and circuit voltage curve open (OCV) estimated)

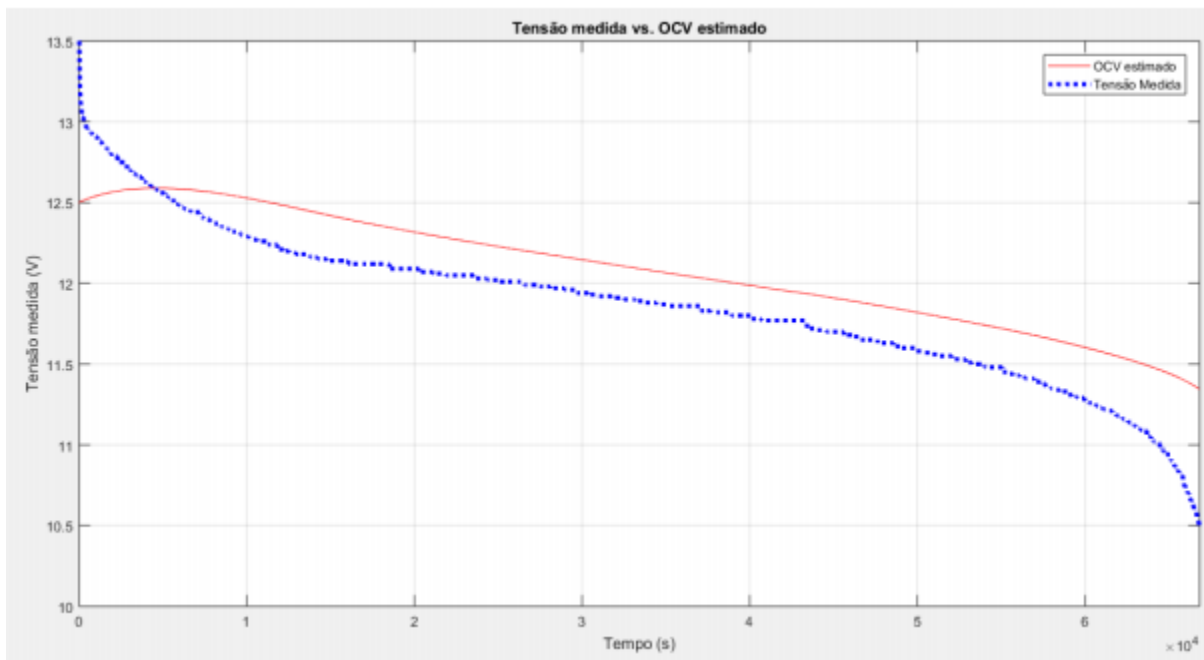


(Fig.7.11 Result of SOC estimation simulation per Kalman filter with data from a C20 discharge)

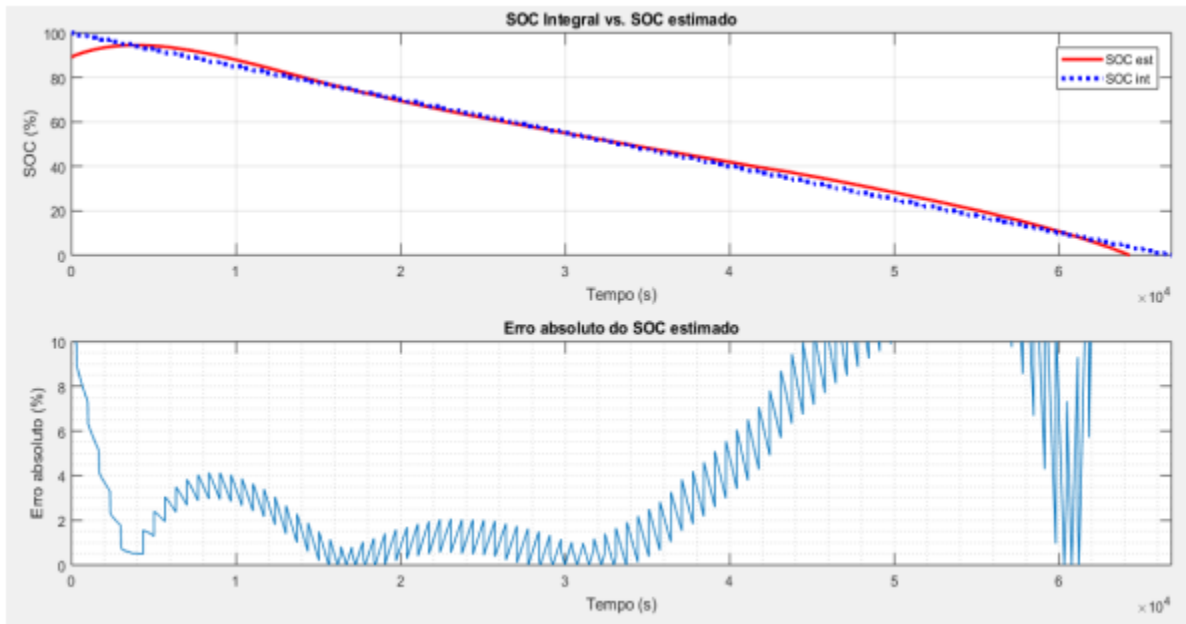
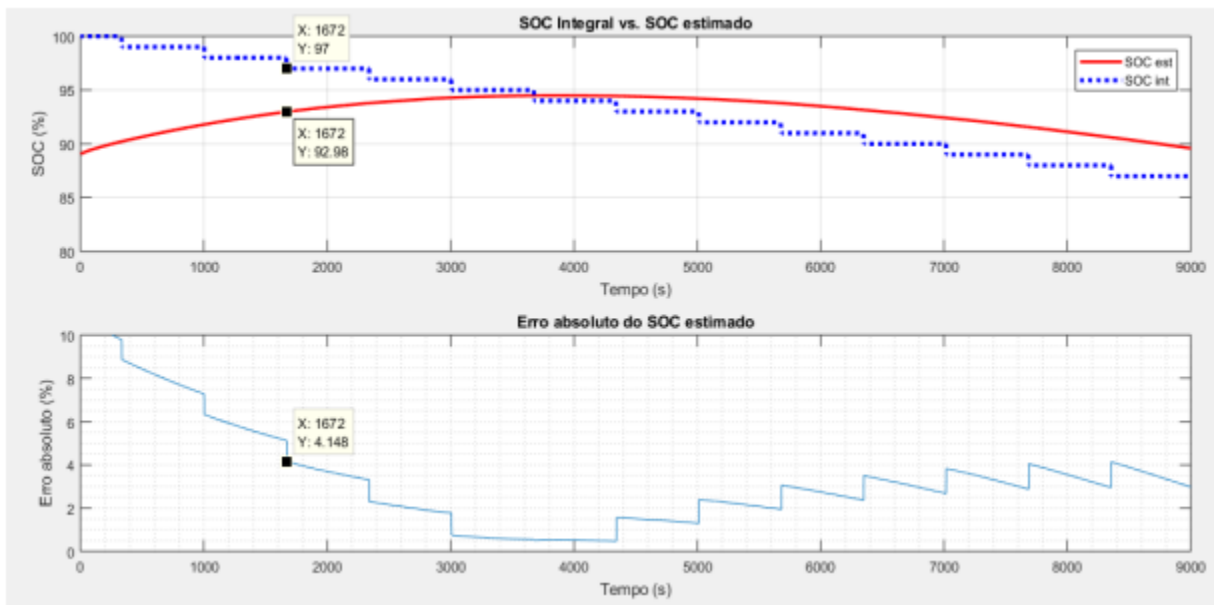


(Fig.7.12 Detail of filter stabilization time)



7.2.2 Field Results

The remote monitoring electronic circuit was used to record the battery's electrical data, such as voltage and current, and ambient temperature data in the isolated photovoltaic system. From

this data, the circuit estimates the battery's SOC, stores it in memory and presents it in time. The actual in a liquid crystal display together with relevant set information such as battery voltage and current, ambient temperature, date and time.

Before being installed on the solar pole, the monitoring system was evaluated for its energy consumption to check the impact of its insertion in the photovoltaic system. The circuit had an average consumption of 200mA. This consumption was recorded with the liquid crystal display on and with its retro lighting activated. The display was only necessary when some query in time real needed to be performed on the spot, which was not a routine situation after the installation of the system on the pole. In this way, a key was installed for activation of the display only when necessary. With the display off, the consumption of the device has been reduced to 140mA. This is the average total system consumption when the GSM/GPRS module is in standby mode. At the time of communication, peaks of up to 300mA could be observed only in the consumption of the GSM/GPRS module, however, the peaks last only 2 seconds and represent an impact not very significant for the average total consumption of the system.

The records of battery voltage and current during a given periods of October and November of 2018 are presented, respectively, in **Figure 7.13** and **Figure 7.14**. In Figure 7.13 the battery voltage is presented. In it, two periods of the day where fundamental situations for the longevity of the battery in the isolated photovoltaic system occur stand out, namely, the end of discharge voltage, approximately 12.47V, that is, the battery voltage in the end of the night; and the fluctuation voltage, for which the charge controller lowers the voltage after the battery reaches approximately 14.2V, as a way to avoid overcharging and consequent loss of water in the battery, thus extending its useful life (PINHO; GALDINO, 2014).

It is observed that, for the period evaluated, the tension at the end of the night was repeating itself around the value of 12.47V, arising the hypothesis that the battery was being fully recharged daily, avoiding deep discharge at each daily cycle. To validate this hypothesis, battery recharge data in the laboratory were evaluated and confronted with the field data.

Figure 7.15 shows the current curve and the curve of the ratio between the amount of charge available at recharging and the amount of charge removed at previous discharge. The data are from a laboratory recharging with duration of 24 hours, current limited to 25A and voltage limited to 14.4V. It was observed that approximately the twenty-second hour of recharging the current stabilized in the value of 2A. According to the battery manufacturer, when the current is stabilized for a period of two hours or longer, during recharging, the battery is fully charged. This battery status could be confirmed by curve of the percentage load available during recharging, where a surplus of about 12% was observed in relation to the amount of cargo removed from the battery at the discharge that preceded it. The theoretical Coulombic efficiency of a lead-acid battery is approximately 95% (PINHO; GALDINO, 2014), Therefore, it was perceived that the 12% available percentage load surplus charging was enough to bring the battery to full state load.

Confronting the above conclusions with the field current data, shown in **Figure 7.14** and **Figure 7.16**, it was observed that the battery stabilized the current of 0,3A for a period of more

than two hours, which confirmed the hypothesis that the battery was, daily, experiencing full recharging.

Figure 7.16 shows the current of the battery during the period chosen from the field collection. The moments of loading and unloading of the battery. During the discharge, the drained battery current was 1.4A, which was used to power the LED fixture during the night. During the day, the variation of the battery charging current occurring according to the variation of the radiation solar module that reached the photovoltaic module on the respective day. The current reached values of peak of the order of 7A. Figure 7.2.2.4 helped to note that at the time the battery reached maximum voltage, between 14V and 14.4V, and was submitted to voltage of fluctuation, around 13.6V, the current was reduced considerably; from that the natural gasification process inside the battery was intensified (PINE; GALDINO, 2014).

Again, comparing the field data with the laboratory data, Figure 7.15 made it easier to see when gasification was intensifying. It was observed that, at the beginning of the recharging, the current remained constant at the maximum value established in the test, in this case, 25A. The linear curve of the available percentage charge amount (current integration) indicated that practically all the current supplied to the battery was being consumed to restore its capacity. In this phase of constant current between 80% and 90% of battery capacity (PINHO; GALDINO, 2014).

(Fig. 7.13 Tension data collected between October and November 2018)

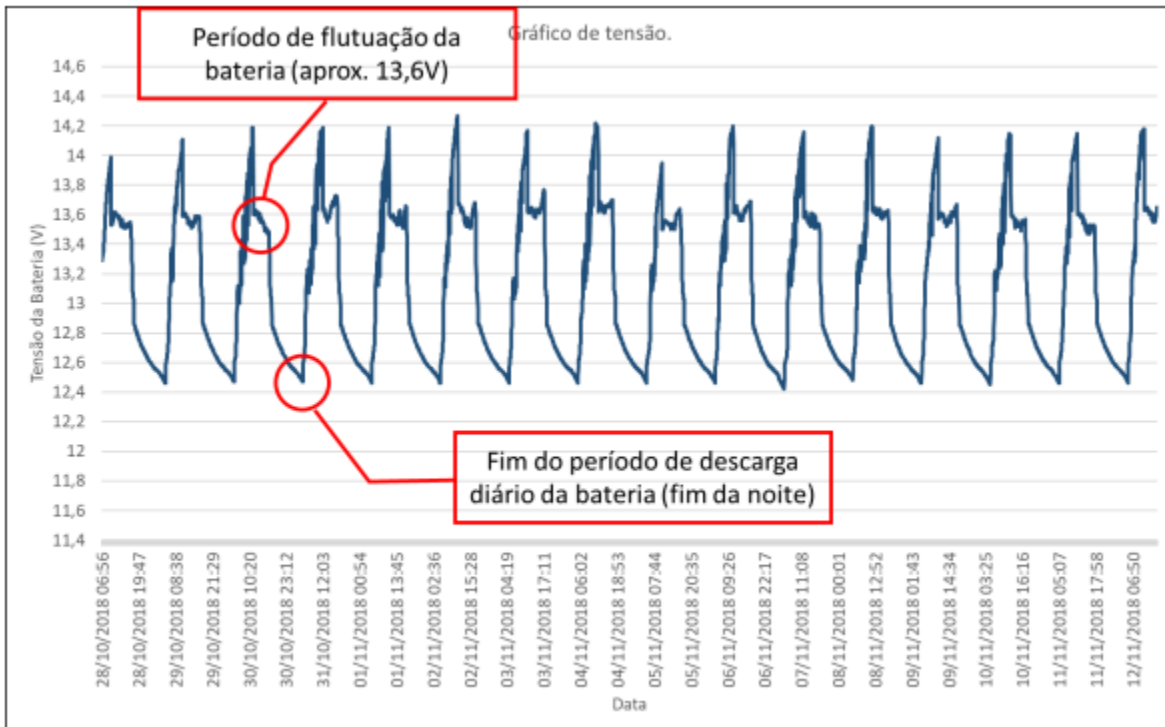


(Fig. 14 Current data collected in the same period)

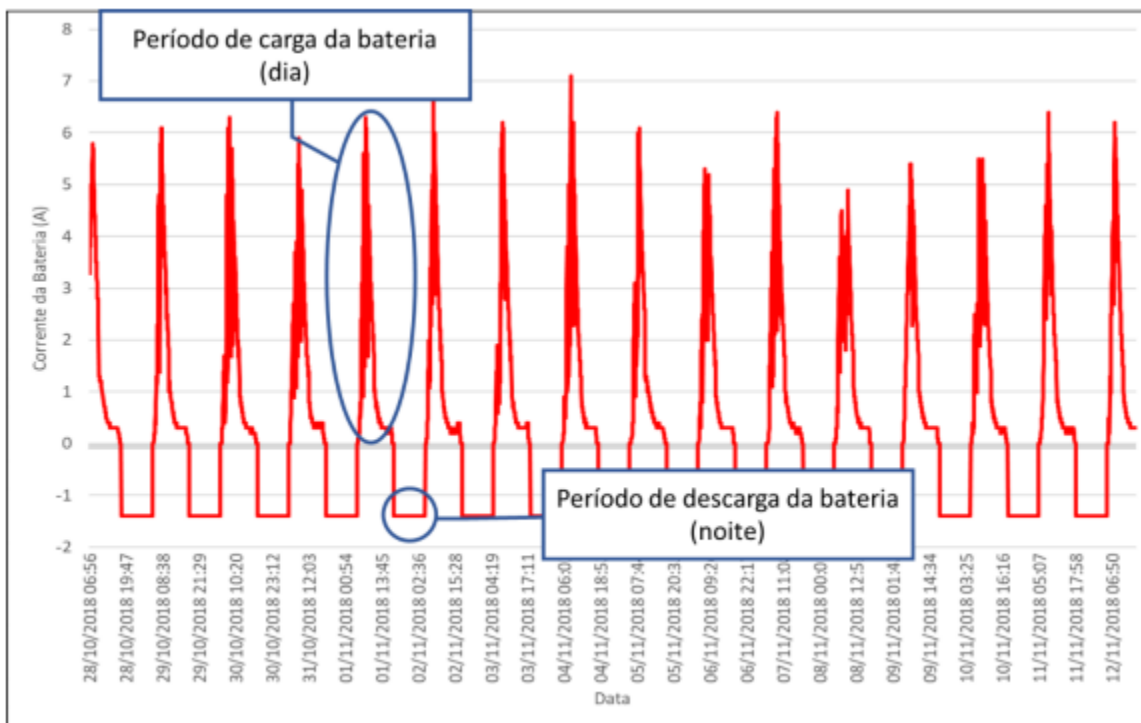


(Fig.7.15 Current Curve and Percentage Charge Amount available for the battery during laboratory recharging)

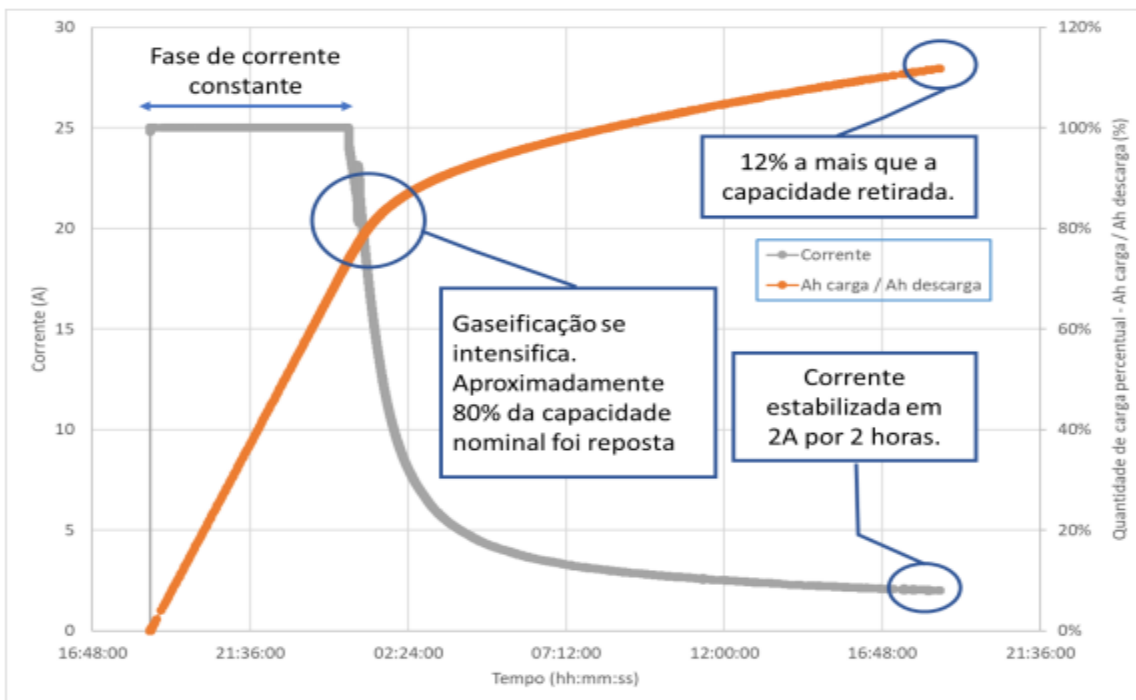
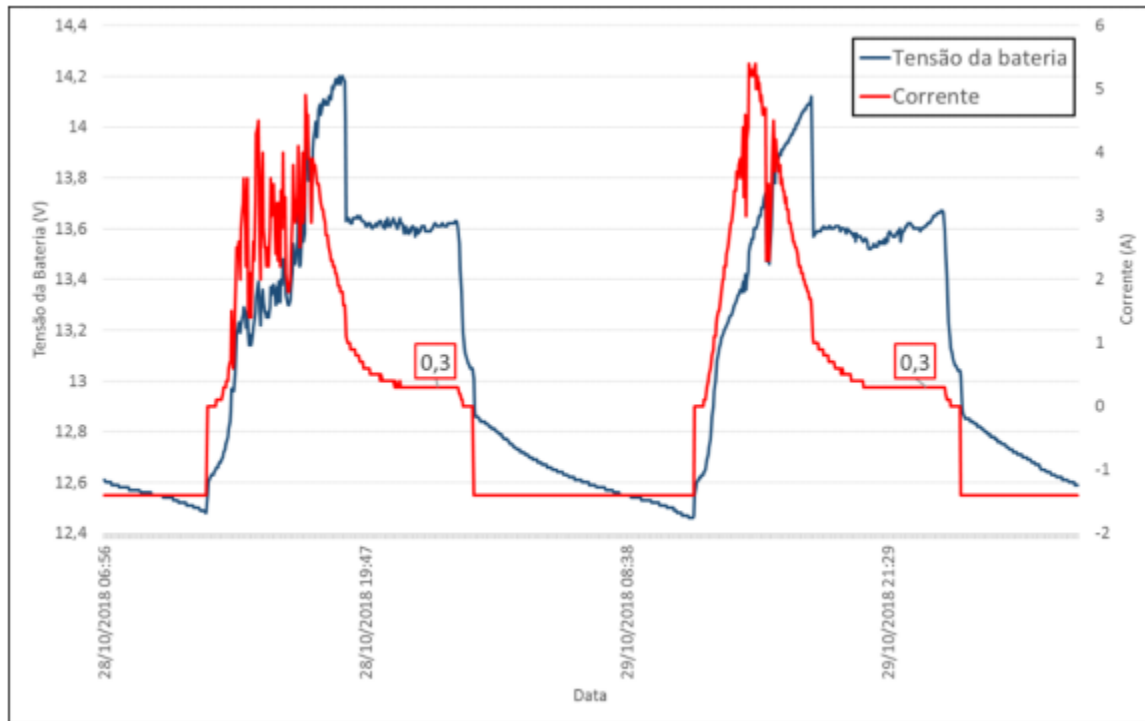


(Fig.7.16 Extended view of two-day current data collection)



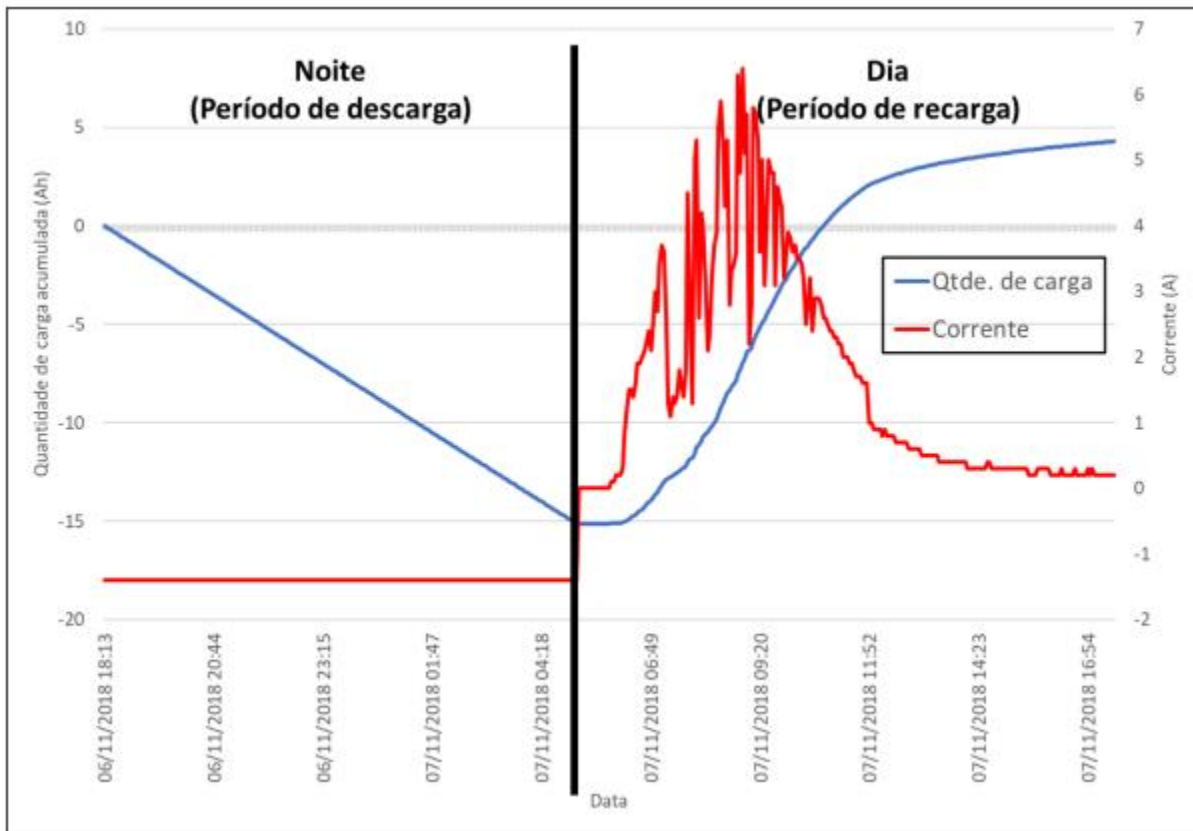
From the point of view of battery charge balance, from the data of the electric current, it was found that the average daily load quantity taken from the battery was 14.80Ah, which represented an average daily minimum SOC of 92.6%, for the period evaluated. For the reload, the available average daily load quantity was 18.42Ah, i.e. approximately 24.5% more of the load consumed was made available to the battery during the period of the day, corroborating with the veracity of the hypothesis that the battery was daily being fully loaded.

Evaluating the battery charge balance data, it was realized that there was an over dimensioning in the solar pole design since it's recommended by the manufacturer to discharge the battery daily until a state of load of 80% of its nominal capacity. For better visualization, [Figure 7.17](#) illustrates the behavior of the cumulative load quantity for one of the days of the collection period. During the battery discharge, i.e. at night, the amount of accumulated charge becomes each more negative due to the direction of the current, coming out of the battery. The opposite happens during the day when the battery is recharged.

The information taken from the data collected in the field, discussed above, served as a reference for the validation of the Kalman filter algorithm which was embedded in the platform-developed remote monitoring system Arduino, whose code is given in Annex D. To facilitate the analysis and visualization, one of the days of the collection period was chosen to present the results. [Figure 7.18](#) presents the result of the SOC estimated by Arduino in real time, compared with the integration method of the chain or Coulomb counting. It was observed that after the stabilization time, the filter started to follow the SOC curve estimated by current integration. A [Figure 7.20](#) shows the absolute SOC error estimated by Arduino when compared to the SOC estimated by the current

integration method. It was observed that the error started at a very high value, over 10%. This was justified for the time needed for the filter to stabilize. After stabilization of the filter, the error had a maximum value of 1.7%, as highlighted in the graph. In Figure 7.18 it is possible to observe that the filter has tended to follow the SOC curve more and more by current integration, generating fewer and fewer errors. At the end of the discharge, that is, at the end of the night, the error was around 0.5%, as highlighted in the graph.

(Fig. 7.17 Behavior of the amount of charge available by the panel during the day and by the battery at night in relation to the nominal capacity of the battery, on one of the days of the collection period)



The message configured for automatic sending via SMS during the download period is simple, however, several other relevant data can be included in the message content, as well as the frequency of sending messages can also be changed to the liking of the receiver, however, one must take into account the peak consumption of the GSM/GPRS module observed when in active communication mode.

The information received makes up a local database on the mobile phone for future queries and assessments of battery and system behavior photovoltaic monitored as a whole. The sending frequency has been set to two-hour intervals in order to mitigate the impact of the consumption of the GSM/GPRS module during the sending of messages.

(Fig.7.18 Comparison between the SOC estimated by Arduino's Kalman filter algorithm and the SOC of the current integration method)

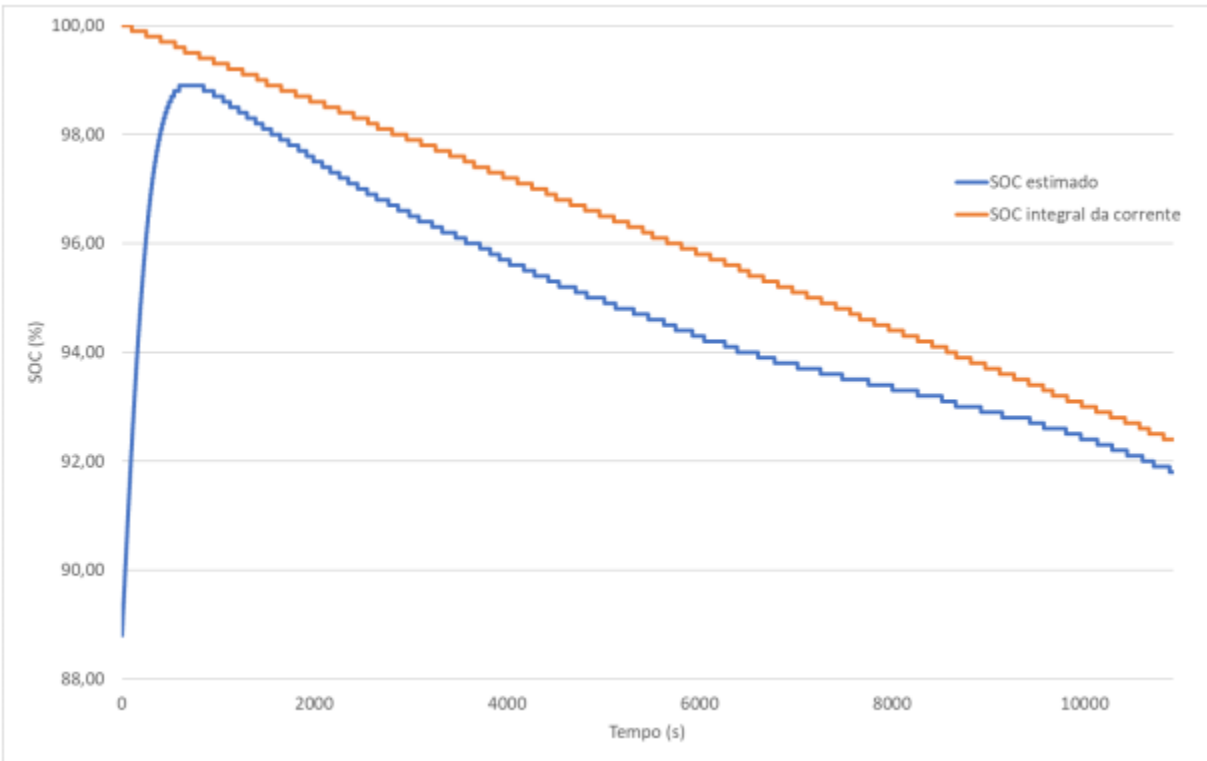


(Fig. 7.19 Kalman filter stabilization time implemented in Arduino)

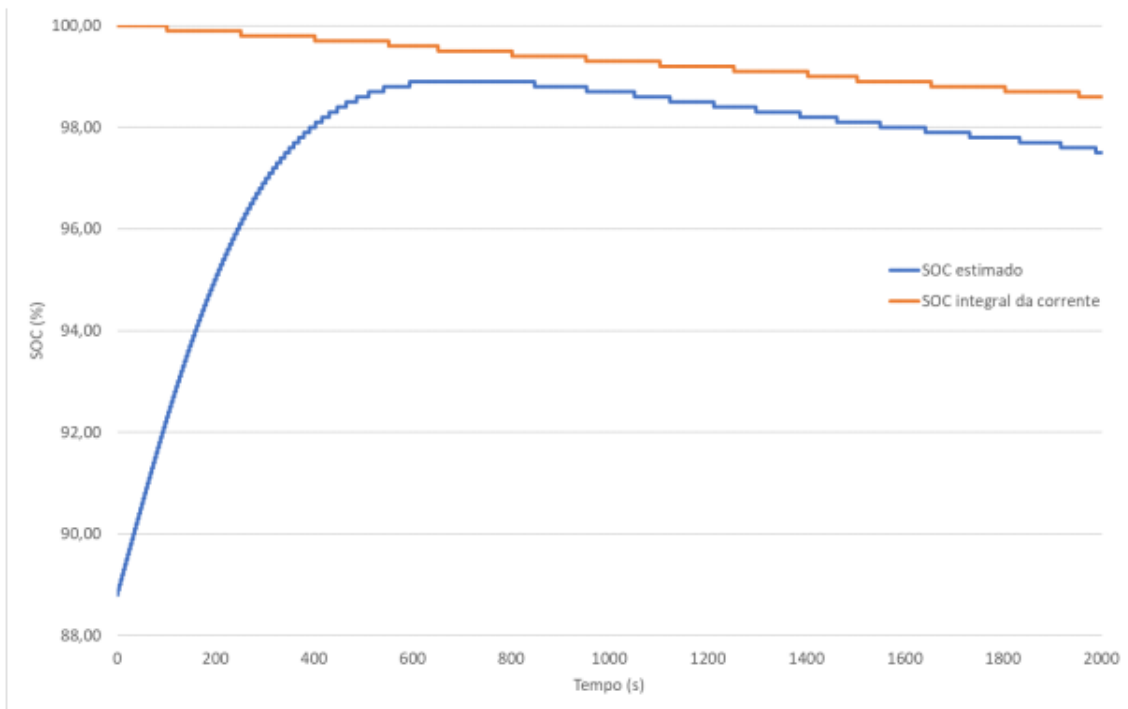


(Fig. 7.20 SOC error by Kalman filter compared to SOC by current integration)

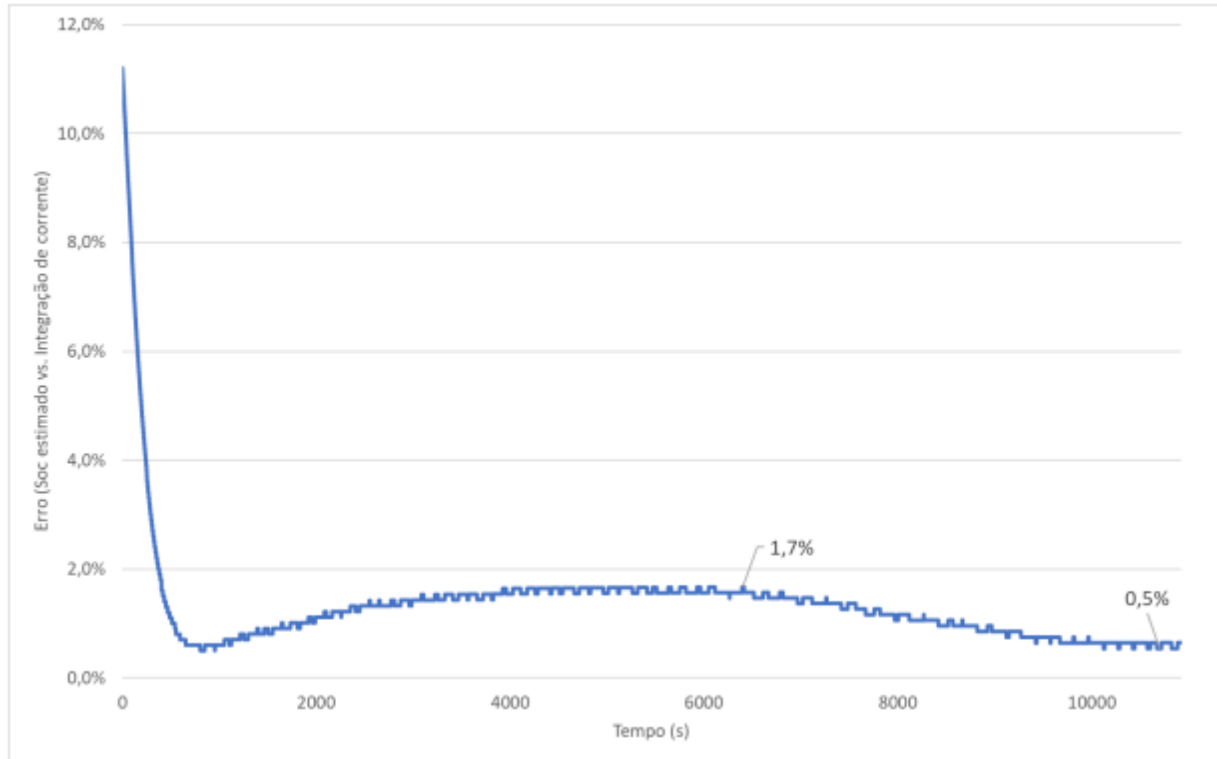
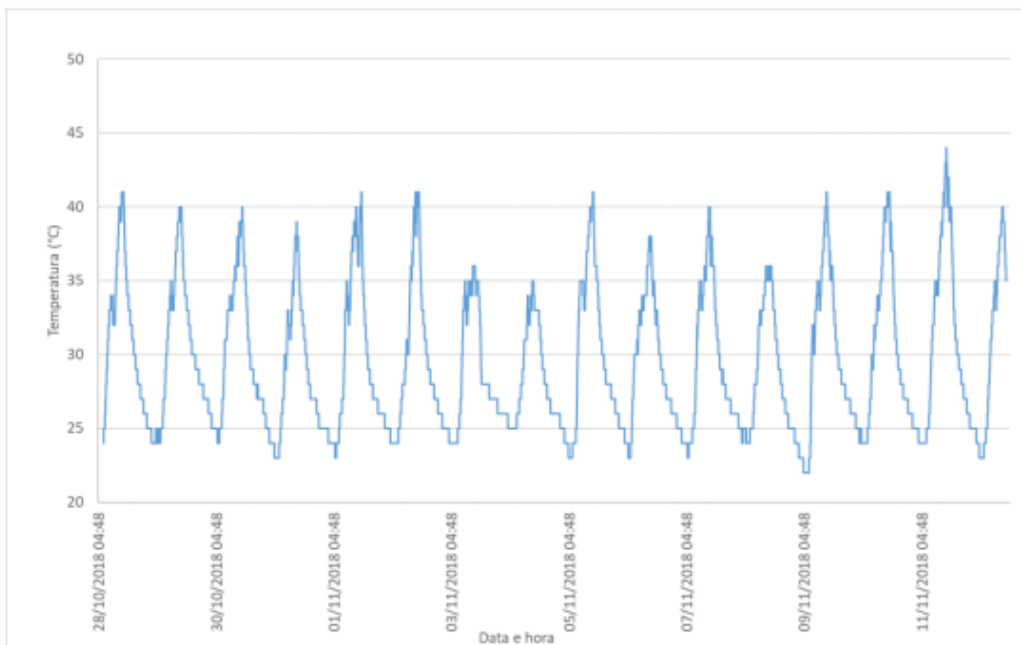


(Fig.7.21 Ambient temperature recorded in the battery compartment during the collection period data)



8 Conclusions

In this work a system for remote monitoring of the state of charge (SOC) of lead-acid ventilated stationary batteries was developed using the Kalman filter technique, for use in isolated photovoltaic systems.

The electronic circuitry developed for battery SOC monitoring has proved to be very stable and reliable. It met the premise of low consumption (140mA) minimizing the impact of its insertion in the photovoltaic system, since its power came from the instrumented battery.

The Kalman filter algorithm implemented in Arduino, when estimating the battery SOC of the isolated photovoltaic system, showed a maximum absolute error of 1.7% between the regions of 100%SOC and 92%SOC, an error that is considerably irrelevant since, even so, it is possible to identify with relative precision the charging and discharging profile to which the battery is being submitted.

The cost benefit of the system developed was quite satisfactory given the R\$550.00 cost of the circuit. This value represents approximately 14% of the value of a commercial datalogger that does not have the battery's SOC estimation function. Currently, this datalogger is used by the battery manufacturer Acumuladores Moura S/A to monitor, locally, its batteries installed in the field.

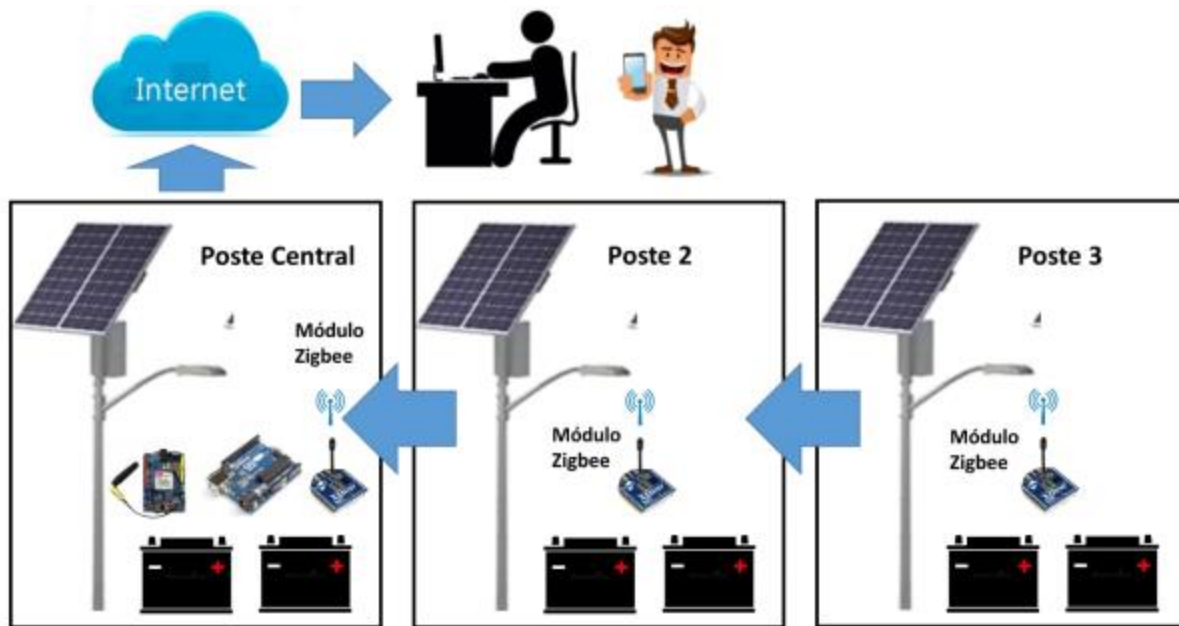
Finally, considering the satisfactory results with the circuit implemented using the Kalman filter technique for battery SOC estimation, the activities presented below will be developed in the future, continuing this work.

In order to further improve the cost benefit system of remote monitoring, the poles will be equipped with radio communicators from Zigbee technology, which enables the creation of a large communication network between devices in mesh topology, i.e. all devices can exchange data between them (DIGI, 2018). This way, only one pole will be equipped with the device complete which is composed by Arduino and the remote communication module GSM/GPRS. Tests will need to be conducted to verify that the distances between the poles are in accordance with the maximum distance limits between the radiocommunications.

Figure 8.1 presents an overview of the battery monitoring system in developing isolated photovoltaic systems. **Figure 8.2** presents an outline of the website layout that will be developed to present the information of each pole through online consultations and will be embedded in the circuitry of the developed device.

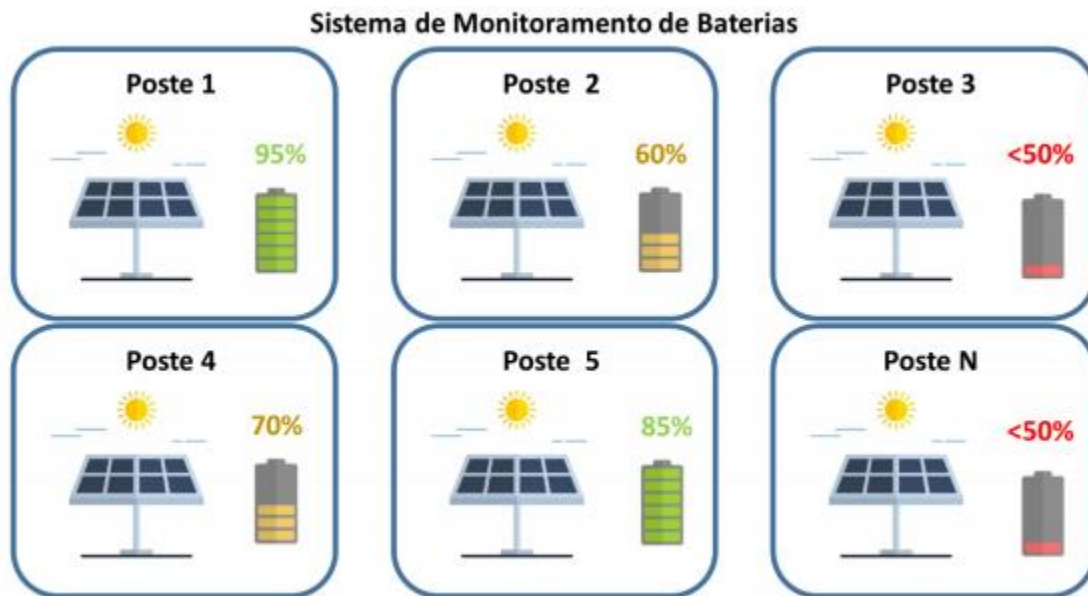
In addition to estimating battery SOC, a State-of-Health (SOH) battery health estimation algorithm will be implemented in the circuit, also using the Kalman filter method.

(Fig.8.1 Overview of the system under development for remote monitoring of batteries in isolated photovoltaic systems)



Source: Writer

(Fig.8.2 Website layout to be developed for remote monitoring of the batteries of isolated photovoltaic systems)



Source: Writer

The following points are suggested for future work:

- Implement SOC estimation by Kalman filter in conjunction with the current integration method or Coulomb counting.
- Battery State of Health measurement using the developed prototype.
- Structure a system similar to the one implemented in this work for systems with voltages above 12V, such as 24V and 48V.
- Study the use of the system implemented in other types of isolated solar photovoltaic systems, such as domestic systems.

9 References

- ANBUKY, Adnan H.; PASCOE, Phillip E. **VRLA battery state-of-charge estimation in telecommunication power systems**. IEEE Transactions on Industrial Electronics, v. 47, n. 3, p. 565-573, 2000.
- BHANGU, B. S. et al. **State-of-charge and state-of-health prediction of lead-acid batteries for hybrid electric vehicles using non-linear observers**. In: Power Electronics and Applications, 2005 European Conference on. IEEE, 2005. p. 10 pp.-P. 10.
- BISHOP, Gary et al. **An introduction to the Kalman filter**. Proc of SIGGRAPH, Course, v. 8, n. 27599-3175, p. 59, 2001.
- BRASIL. Ministério de Minas e Energia. EPE - **Empresa de Pesquisa Energética. Balanço Energético Nacional 2018**. Ano base, 2017. Rio de Janeiro, 2018.
- CHANG, Wen-Yeau. **The state of charge estimating methods for battery: A review**. ISRN Applied Mathematics, v. 2013, 2013.
- CHEN, C. Julian. **Physics of solar energy**. John Wiley & Sons, 2011.
- DA COSTA, Sonia Carina Lopes; ARAUJO, Armando Sousa; DA SILVA CARVALHO, Adriano. **Battery state of charge estimation using extended Kalman filter**. In: 2016 International Symposium on Power Electronics, Electrical Drives, Automation and Motion (SPEEDAM). IEEE, 2016. p. 1085-1092.
- DIGI. Zigbee RF Modules. **XBEE2, XBEEPRO2, PRO S2B**. User Guide, 2018.
- EPEVER. LandStar **EPLI Series Solar Charge Controller**.
- FLUKE. Fluke 500 **Series Battery Analyzers**. Technical Data.
- FONTES, Fernando Antonio de S.; BASTOS, PRFMA. **Experiência com Geração Fotovoltaica no Estado da Bahia**. Proc. 2012 IV Simpósio Brasileiro de Sistemas Elétricos, 2012.
- HARIPRAKASH, B. et al. **Comparative study of lead-acid batteries for photovoltaic stand-alone lighting systems**. Journal of Applied Electrochemistry, v. 38, n. 1, p. 77-82, 2008.
- HUGGINS, Robert. **Advanced batteries: materials science aspects**. Springer Science & Business Media, 2009.
- JENKINS, D. P.; FLETCHER, J.; KANE, David. **Lifetime prediction and sizing of lead-acid batteries for microgeneration storage applications**. IET Renewable Power Generation, v. 2, n. 3, p. 191-200, 2008.
- MARTIN MURNANE, ADEL GHAZEL, " **A Closer Look at State of Charge (SOC) and State of Health (SOH) Estimation Techniques for Batteries**"
- JOHNSON, Valerie H.; PESARAN, Ahmad A.; SACK, Thomas. **Temperature dependent battery models for high-power lithium-ion batteries**. City of Golden: National Renewable Energy Laboratory, 2000.

KAISER, Rudi. **Optimized battery-management system to improve storage lifetime in renewable energy systems.** Journal of Power Sources, v. 168, n. 1, p. 58- 65, 2007.

LOUKIL, Jihen; MASMOUDI, Ferdaous; DERBEL, Nabil. **State of charge estimation of lead acid battery using a Kalman filter.** In: 2017 14th International MultiConference on Systems, Signals & Devices (SSD). IEEE, 2017. p. 308-312.

MARCHILDON, Jacques; DOUMBIA, Mamadou Lamine; AGBOSSOU, Kodjo. **SOC and SOH characterisation of lead acid batteries.** In: IECON 2015-41st Annual Conference of the IEEE Industrial Electronics Society. IEEE, 2015. p. 001442-001446.

MOO, C. S. et al. **State-of-charge estimation with open-circuit-voltage for leadacid batteries.** In: Power Conversion Conference-Nagoya, 2007. PCC'07. IEEE, 2007. p. 758-762.

MORNINGSTAR. **Solar Charging System Controller. Installation, Operation and Maintenance Manual,** 2018. MOURA.

Catálogo de Produtos, 2017. MOURA. Especificações Técnicas. Bateria Moura Clean Modelo 12MF220, 2017. MOURA.

Manual Técnico Baterias Moura Clean Nano, 2016.

NG, Kong-Soon et al. **An enhanced coulomb counting method for estimating state-of-charge and state-of-health of lead-acid batteries.** In: Telecommunications Energy Conference, 2009. INTELEC 2009. 31st International. IEEE, 2009. p. 1-5.

TONOLI, ANDREA, “**Estimation Accuracy and Computational Cost Analysis of Artificial Neural Networks for State of Charge Estimation in Lithium Batteries**”, 2019

NG, Kong-Soon et al. **State-of-charge estimation for lead-acid batteries based on dynamic open-circuit voltage.** In: Power and Energy Conference, 2008. PECon 2008. IEEE 2nd International. IEEE, 2008. p. 972-976.

CRISTEN CONGER; **How can Solar Panels Power a Car.** 2018

PRABHAKAR, Bhavya M.; RAMPRABHAKAR, J.; SAILAJA, V. **Estimation and controlling the state of charge in battery augmented photovoltaic system.** In: 2016 Biennial International Conference on Power and Energy Systems: Towards Sustainable Energy (PESTSE). IEEE, 2016. p. 1-6.

ALEXANDRE, Laurent; **Different Types of Electric Car Batteries,** 2019

RHUDY, Matthew B.; SALGUERO, Roger A.; HOLAPPA, Keaton. **A Kalman Filtering Tutorial For Undergraduate Students.** International Journal of Computer Science & Engineering Survey (IJCSES), v. 8, p. 1-18, 2017.

SAUER, Dirk Uwe. **Electrochemical storage for photovoltaics.** Handbook of photovoltaic science and engineering, p. 896-953, 2011.

SATO, Shinya; KAWAMURA, Atsuo. **A new estimation method of state of charge using terminal voltage and internal resistance for lead acid battery.** In: Power Conversion Conference, 2002. PCC-Osaka 2002. Proceedings of the. IEEE, 2002. p. 565-570.

WATRIN, Nicolas; BLUNIER, Benjamin; MIRAOUI, Abdellatif. **Review of adaptive systems for lithium batteries state-of-charge and state-of-health estimation.** In: Transportation Electrification Conference and Expo (ITEC), 2012 IEEE. IEEE, 2012. p. 1-6.

ZHAO, Bo et al. **Operation optimization of standalone microgrids considering lifetime characteristics of battery energy storage system.** IEEE transactions on sustainable energy, v. 4, n. 4, p. 934-943, 2013.

KALOGIROU, Soteris A. **Solar energy engineering: processes and systems.** Academic Press, 2013.

KYOCERA. **High efficiency multi-crystalline photovoltaic module - KD250GH4FB2.**

Annex A: Technical specifications of the solar pole components

Tabela A.1 – Especificações técnicas do módulo fotovoltaico do poste solar.

Parâmetro	Especificação (@1000W/m²)
Fabricante	Kyocera
Modelo	KD250GH-4FB2
Potência máxima	250W
Tensão de máxima potência	29,8V
Corrente de máxima potência	8,39A
Tensão de circuito aberto	36,9V
Corrente curto-circuito	9,09A
Eficiência	15,1%

Fonte: Kyocera

Tabela A.2 – Especificações técnicas da luminária do poste solar.

Parâmetro	Especificação
Fabricante	Alper
Modelo	ALP-LPT4-30W
Potência	30W

Tabela A.3 – Especificações técnicas do controlador de carga do poste solar.

Parâmetro	Especificação
Fabricante	Epever
Modelo	LS2024100EPLI
Tensão nominal do sistema	12/24VDC Auto
Máxima corrente de carga	10A
Max. tensão de circuito aberto do módulo	50V
Tensão de entrada da bateria	9~32V
Max. Potência de saída	50W/12V;100W/24V
Max. corrente de saída	3,3A
Tensão máxima de saída	Max. tensão da bateria +2V~60V
Tensão de circuito aberto da carga	60V
Eficiência	96%
Precisão no controle da corrente de saída	≤30mA
Tipo de bateria	Sealed(Default) / Gel / Flooded / User
Auto consumo	≤9,1mA(12V); ≤7,0mA(24V)
Coeficiente de compensação da temperatura	-3mV/°C/2V
Temperatura ambiente de trabalho	-35°C~+55°C

Tabela A.4 – Especificações técnicas da bateria de chumbo-ácido estacionária ventilada utilizada no poste solar.

Parâmetro	Especificação
Fabricante	Moura
Modelo	12MF220
Tensão nominal	12V
Temperatura de referência	25°C
Máxima temperatura de trabalho	65°C
Mínima temperatura de trabalho	-10°C
Vida útil estimada	4 anos (20% DOD)
Tensão de flutuação	13,5V
Tensão de carga	14,7V
Tensão de equalização	15,4V (realizar a cada 28 dias)
C10 Nominal (1,75Vpe, 25°C)	200Ah
C20 Nominal (1,75Vpe, 25°C)	220Ah
Dimensões (C x L x A)	517mm x 272mm x 246mm
Peso	57,8kg

Annex B: Technical specification of cycling equipment

Tabela B.1 – Especificações do equipamento de carga e descarga automática de baterias do fabricante Digatron.

Parâmetro	Especificação
Fabricante	Digatron
Modelo	UBT-0/18-30
Quantidade de circuitos	30
Corrente	0,03 a 30,00A ($\pm 0,01A$)
Tensão	0,005 a 18,000 ($\pm 0,001V$)
Resolução	15bits

Fonte: Digatron

Annex C: Kalman Filter MATLAB Algorithm

```
%%%%%%%%%%%%%%%%%%%%%%%%%%%%%%%%%%%%%%%%%%%%%%%%%%%%%%%%%%%%%%%%%%%%%%%% FILTRO DE KALMAN %%%%%%%%%%%%%%%%%%%%%%%%%%%%%%%%%%%%%%%%%%%%%%%%%%%%%%%%%%%%%%%%%%%%%%%%%
Q = [10e-8, 0, 0;
     0, 10e-8, 0;
     0, 0, 10e-8];
R = 12e3;

%%%% Valores estimados iniciais %%%%
x_est = (13.1; 13.1; 13.1);
p_est = (1, 0, 0; 0, 1, 0;
         0, 0, 1);

%%%% Inicializando vetores %%%%
Vbulk = zeros (1, length(tensao));
y = zeros (1, length(tensao));
soc_est = zeros (1, length(tensao));
Vterminal = zeros (1, length(tensao));
erro = zeros (1, length(tensao));

%%%% Valores preditos %%%%
for i = 1: length(tensao);
    x_prd = Ad * x_est + Bd * u;
    p_prd = Ad * p_est * Ad' + Q;
    %%%% Valores estimados %%%%
    num = p_prd * H';
    den = H * p_prd * H' + R;
    kalman_gain = num/den;
    x_est = x_prd + kalman_gain * (tensao(i) - H * x_prd);
    p_est = p_prd - p_prd * kalman_gain * H;
    Vbulk(i) = x_est(1,1); % OCV
    Vterminal(i) = x_est(3,1);
end
```

end

Annex D: Kalman Filter Arduino Algorithm

```
//////////Cálculo do x_predito
for(col = 0; col < 1; col++) {
  for(lin = 0; lin < 3; lin++){
    for(i = 0; i < 3; i++){
      mult = A(lin)(i) * x_estimado(i)(col);
      mult_acu = mult_acu + mult; }

    x_predito(lin)(col) = mult_acu + (B(lin)(col))*corrente;
    mult = 0;
    mult_acu = 0; }}

```

```
//////////Cálculo do P_predito
for(col = 0; col < 3; col++) {
  for(lin = 0; lin < 3; lin++) {
    for(i = 0; i < 3; i++){
      mult = A(lin)(i) * P_estimado(i)(col);
      mult_acu = mult_acu + mult; }

    A_mult_Pest(lin)(col) = mult_acu;
    mult = 0;
    mult_acu = 0; }}

```

```
for(col = 0; col < 3; col++) {
  for(lin = 0; lin < 3; lin++){
    for(i = 0; i < 3; i++){
      mult = A_mult_Pest(lin)(i) * AT(i)(col);
      mult_acu = mult_acu + mult; }

```

```
A_mult_Pest(lin)(col) = mult_acu;
mult = 0;
mult_acu = 0; }}

```

```
for(col = 0; col < 3; col++) {
  for(lin = 0; lin < 3; lin++){
    for(i = 0; i < 3; i++){
      mult = A_mult_Pest(lin)(i) * AT(i)(col);
      mult_acu = mult_acu + mult; }

    P_predito(lin)(col) = mult_acu + Q(lin)(col);
    mult = 0;
    mult_acu = 0; }}

```

//////////Cálculo do ganho do filtro de Kalman

```
for(col = 0; col < 1; col++){  
  for(lin = 0; lin < 3; lin++){  
    for(i = 0; i < 3; i++){  
      mult = P_predito(lin)(i) * HT(i)(col);  
      mult_acu = mult_acu + mult; }  
  
    Ppred_mult_HT(lin)(col) = mult_acu;  
    mult = 0;  
    mult_acu = 0; }}
```

```
for(col = 0; col < 1; col++) {  
  for(lin = 0; lin < 1; lin++) {  
    for(i = 0; i < 3; i++){  
      mult = H(lin)(i) * Ppred_mult_HT(i)(col);
```

```
      mult_acu = mult_acu + mult; }
```

```
      H_Ppred_HT_R = mult_acu + R;  
      mult = 0;  
      mult_acu = 0; } }
```

```
for(lin = 0; lin < 3; lin++){  
  Ganho_Kalman(lin)(0) = (Ppred_mult_HT(lin)(0)) / H_Ppred_HT_R; }
```

```
for(col = 0; col < 1; col++) // Matriz x_predito eh 3x1{  
  for(lin = 0; lin < 1; lin++) {  
    for(i = 0; i < 3; i++){  
      mult = H(lin)(i) * x_predito(i)(col);  
      mult_acu = mult_acu + mult; }
```

```
    inovacao = tensao_medida - mult_acu;  
    mult = 0;  
    mult_acu = 0; }}
```

```
for(lin = 0; lin < 3; lin++){  
  x_estimado(lin)(0) = x_predito(lin)(0) + (Ganho_Kalman(lin)(0)) * inovacao; }
```

```
for(col = 0; col < 3; col++) // Matriz H eh 1x3{  
  for(lin = 0; lin < 3; lin++) {  
    for(i = 0; i < 1; i++){  
      mult = Ganho_Kalman(lin)(i) * H(i)(col);  
      mult_acu = mult_acu + mult; }
```

```
I_K_H(lin)(col) = identidade(lin)(col) - mult_acu;  
mult = 0;  
mult_acu = 0; }}
```

```
for(col = 0; col < 3; col++){  
  for(lin = 0; lin < 3; lin++) {  
    for(i = 0; i < 3; i++){  
      mult = I_K_H(lin)(i) * P_predito(i)(col);  
      mult_acu = mult_acu + mult; }  
    }
```

```
  P_estimado(lin)(col) = mult_acu;  
  mult = 0;  
  mult_acu = 0; }}}}
```

Annex E: Electronic Circuit Scheme to Monitor the Battery

